Iranian Journal of Basic Medical Sciences
ijbms.mums.ac.ir

Ultrasound medicine in the era of precision theranostics: Mechanisms, molecular strategies, and clinical translation

Lei Wang [1], Zhiyu Luo [1]*, Dan Liu [2]

[1] Affiliated Hospital of Jinggangshan University, Ji'an Jiangxi, 343000, China
[2] Jinggangshan University, Ji'an Jiangxi, 343009, China

ARTICLE INFO

Article type:
Review

Article history:
Received: Aug 21, 2025
Accepted: Oct 26, 2025

Keywords:
High-intensity focused-ultrasound
Low-intensity pulsed-ultrasound
Molecular imaging
Sonoporation
Theranostics
Ultrasound

ABSTRACT

Ultrasound (US) has evolved from a solely diagnostic tool into a multifaceted theranostics platform, proficient in both high-resolution imaging and tailored therapeutic intervention. Progress in acoustic physics, microbubble and nanobubble technology, and precision beam-forming has broadened its applications in cancer, neurology, cardiovascular diseases, and regenerative medicine. Notwithstanding these advancements, the translation into conventional clinical procedures is impeded by inadequate mapping of acoustic thresholds, variable safety factors, and insufficient integration with molecular and immunological targeting techniques, such as limited ligand specificity, off-target effects, and inconsistent activation of immune responses. This study consolidates the present knowledge of the mechanical, thermal, and sonochemical processes involved in US tissue interactions, focusing on controlled cavitation, bioheat transfer, and the formation of reactive oxygen species. We investigate novel molecular techniques such as ultrasound-targeted drug delivery, gene therapy, immunomodulation, and sonodynamic treatment, emphasizing significant preclinical and clinical achievements. The exploration of cross-modality synergies, including magnetic resonance imaging, photoacoustic imaging, and nuclear medicine, demonstrates how US might enhance current diagnostic and therapeutic processes. Particular emphasis is centered on the tumor microenvironment, where US may influence immune cell migration, destroy stromal barriers, and augment the effectiveness of checkpoint inhibitors. In regenerative medicine, low-intensity pulsed ultrasound (LIPUS) is assessed for its function in mechanotransduction and tissue healing.

▶ Please cite this article as:
Wang L, Luo Zh, Liu D. Ultrasound medicine in the era of precision theranostics: Mechanisms, molecular strategies, and clinical translation. Iran J Basic Med Sci 2026; 29:

Introduction

Because it provides a unique combination of focused treatment potential, live imaging capacity, and a solid safety profile, ultrasound (US) has emerged as a crucial modality in modern healthcare. It transmits non-ionizing mechanical waves that deeply penetrate tissues, setting it apart from other energy-based technologies and enabling a variety of therapeutic approaches in addition to high-accuracy diagnostics. The US has been transformed from a traditional imaging technique into a sophisticated theranostics system that is now essential in areas like tissue regeneration, neurological disorders, cardiovascular medicine, and cancer treatment, thanks to advancements in acoustic design, contrast-enhancing bubble agents, and molecular imaging integration (1, 2).

From a post-World War II experimental curiosity to a vital part of modern healthcare, ultrasonography has evolved over the last 70 years from a merely observational imaging tool to a dynamic technology that can actively affect biological processes (3, 4). Inspired by sonar systems, ultrasonography was first limited to simple A-mode applications for identifying structural defects in the 1940s and 1950s. The discipline was transformed over the next 20 years by innovations such as B-mode imaging and Doppler methods, which enabled real-time visualization of physiological activity and significantly increased its therapeutic relevance (5, 6). US is a key player in theranostics today, combining imaging, molecular-scale monitoring, and precision-guided therapies into a single, integrated therapeutic procedure (7, 8).

The production, transmission, and interaction of high-frequency mechanical waves, typically between 1 and 15 MHz in clinical settings, are the foundation of US, which has its roots in acoustic physics. However, sophisticated systems can function at much higher or lower frequencies for specific applications (9). Variations in acoustic impedance at the tissue-type borders control the behavior of these waves as they travel through biological tissues via reflection, refraction, scattering, and absorption (10). The equilibrium between image resolution and penetration depth is shaped by this physics-biology interaction, with direct therapeutic importance. For this reason, a physician may choose to use a low-frequency transducer to examine deeper abdominal tissues or a high-frequency probe to visualize superficial blood vessels in exquisite detail (11). Notably, the same acoustic principles also underpin therapeutic applications, enabling sub-millimeter-precision energy focus to create controlled mechanical, thermal, or cavitational effects

***Corresponding author:** Zhiyu Luo. Affiliated Hospital of Jinggangshan University, Ji'an Jiangxi, 343000, China. Email: Zhiyu.luo1200@gmail.com

within specific target tissues (12, 13).

Most modern US systems fall into one of three categories: hybrid, therapeutic, or diagnostic. Diagnostic methods include B-mode, M-mode, continuous, pulsed, and color Doppler techniques, as well as elastography, all of which utilize distinct acoustic signal qualities to evaluate the mechanical, structural, and mobility features of tissue (14, 15). Therapeutic US encompasses a wide variety of procedures, including microbubble-assisted sonoporation to enable targeted medication and gene delivery, low-intensity pulsed US to encourage tissue healing, and high-intensity focused ultrasound (HIFU) for accurate tumor eradication (4, 16). The most recent development in US technology is represented by hybrid systems, which combine contemporaneous therapeutic capabilities with high-resolution imaging to provide real-time, feedback-guided therapy. This integrated method enables a single transducer to manage diagnosis, intervention, and monitoring in a single session, shifting the workflow from a sequential "see then treat" model to a unified "see and treat" approach.

US has a special edge in the field of energy-based medical technology. US provides mechanical energy that can be precisely focused deep within the body, without the dangers of ionizing radiation, unlike lasers, which use coherent electromagnetic light, or radiofrequency and microwave devices, which produce heat through dielectric interactions (17, 18). Significant safety and legal advantages result from this, particularly for vulnerable populations like expectant mothers and infants. Furthermore, US often uses the body's own tissue properties to provide its diagnostic contrast, which simplifies processes and reduces expenses in comparison to many electromagnetic-based methods that rely on external chromophores or conductive mediums. US's position as a vital tool in both high-tech clinical facilities and healthcare settings with limited resources has been cemented by its mobility, cheap equipment cost, and smooth integration into point-of-care workflows (5, 8). The absolute novelty of US in the twenty-first century lies in its integration with other scientific fields rather than in incremental improvements in transducer performance or picture quality. The functional limits of the technology are being pushed to new heights by developments like automated image processing powered by artificial intelligence, nanoscale contrast agents for molecular-level vision, and hybrid techniques that combine US with optical or magnetic modalities (11, 13, 16). These developments have made US a versatile platform technology that can be used for various therapeutic purposes, including regenerative medicine and highly focused cancer treatments (4, 7, 19).

This review has a purposefully integrated stance. Few studies combine US's historical evolution, acoustic principles, system classifications, and comparisons with other modalities into a unified, coherent framework. At the same time, much research concentrates only on specific US methods or discrete clinical applications (3, 4, 7, 8). In this study, we bridge these fields to demonstrate how a thorough understanding of US's fundamental underpinnings influences both its current clinical use and its potential for future translation. We illustrate the US's unique benefits, intrinsic limitations, and uncharted territory by placing it within the framework of both rival and complementary energy-based technologies (10, 12). This work has two objectives. First, to trace the development of US medicine from its beginnings in the middle of the 20th century to its present status as a multimodal, hybrid technology that exemplifies the theranostics paradigm (4, 7). To identify critical areas where US might address unsolved issues in diagnosis, treatment, and patient monitoring, our second goal is to critically assess the innovation potential at the intersection of physics, engineering, and clinical practice (11, 13, 16). Our objective is to provide academics, physicians, and engineers with a standard knowledge base that may spur the creation of the next wave of US-driven breakthroughs by tracking its progress and contextualizing it within the broader range of biomedical energy technologies (19).

Ultrasound has been a mainstay of diagnostic medicine since its clinical rise in the mid-20th century, initially used for fetal imaging, transthoracic echocardiography, and Doppler blood flow measurement. Over time, advances such as contrast-enhanced probes, HIFU, and microbubble/nanoparticle carriers have expanded their functionality, enabling not only imaging but also therapeutic modulation of tissues. However, recent years have witnessed a more rapid transformation. Integration of artificial intelligence has enabled automated interpretation of sonograms, AI-guided interventional tools that assist non-expert operators, and segmentation/deep-learning models embedded into portable ultrasound systems to derive functional metrics in real time. Meanwhile, wearable ultrasound devices have emerged, including flexible patches and wireless transducer arrays, capable of deep-tissue monitoring under motion, long-term muscle activity tracking, and continuous respiratory or cardiovascular monitoring. These devices often incorporate AI/ML to interpret the rich signal data. Together, these developments signal a shift from static, operator-dependent imaging toward dynamic, adaptive, personalized theranostics. Yet challenges remain in ensuring robust performance across diverse patient populations, maintaining signal fidelity under motion, achieving long operational lifetimes in wearable formats, and obtaining regulatory and clinical validation for safe translation.

In light of this, we offer ultrasound as a dynamic, highly adjustable platform whose integrative potential will maintain its relevance at a time when intelligent, multipurpose, and minimally intrusive medical instruments are in high demand rather than as a fixed, fully developed technology. With the ability to sense, analyze, and carry out therapeutic activities in real time, it may progress over the next ten years from being one of multiple imaging alternatives to acting as the main control center of image-guided therapies (Figure 1)(4, 7, 20).

Molecular and cellular mechanisms

Mechanical effects

The term "mechanical effects" describes the non-thermal mechanisms by which ultrasound interacts with tissue, primarily via cavitation involving gas bodies, acoustic streaming, and acoustic radiation force. These occurrences, which each have distinct biological impacts and safety implications, may happen in both diagnostic and therapeutic contexts (21, 22).

By transferring momentum to tissue, radiation force creates displacements at the micrometer scale that disclose mechanical characteristics. This idea is the foundation of contemporary elastography methods, such as shear-wave

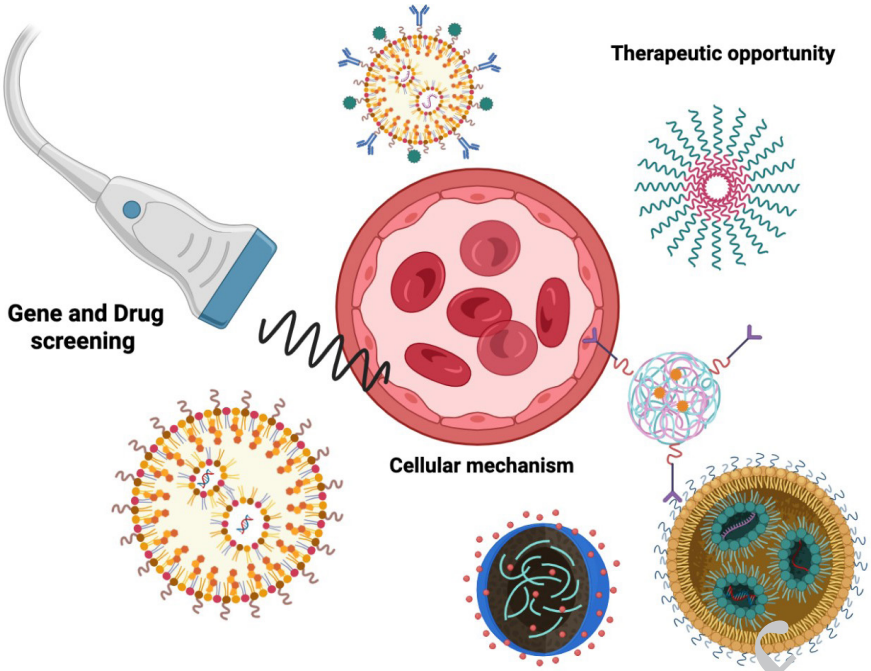

Figure 1. Schematic representation of high-intensity focused ultrasound (HIFU) in cancer therapy
HIFU serves as a versatile platform encompassing three main domains: screening and identifying effective genes or drugs, elucidating underlying cellular and molecular mechanisms, and advancing therapeutic strategies to improve treatment outcomes

elasticity imaging and Acoustic Radiation Force Impulse (ARFI) imaging, which provide quantitative stiffness maps that are now often used in vascular, thyroid, liver, and breast diagnostics (23-26). When evaluating the safety of radiation-force imaging, exposure limits established for brief diagnostic pulses must be used carefully, as these modalities employ longer and higher-intensity pulses than typical B-mode (27). The oscillation of gas bodies caused by an acoustic field is known as cavitation. When bubbles are stable, they show sub- or ultra-harmonic oscillations that produce microstreaming and shear forces that may temporarily change intercellular connections and cell membranes. Rapid bubble collapse in its inertial form may produce wideband acoustic emissions and high-velocity jets, which might harm parenchymal tissue or vascular systems (28, 29). Through transient breaches of cell membranes and endothelial barriers, encapsulated microbubbles facilitate sonoporation, promoting the transfer of medicines and genes by lowering the acoustic threshold for cavitation and limiting mechanical impacts on the microvascular environment (30, 31). Stable cavitation is utilized in conjunction with targeted ultrasound and microbubbles in the central nervous system to temporarily and reversibly break the blood-brain barrier (BBB). Accurate dosage management and real-time safety monitoring are made possible by the connection between acoustic emissions and BBB permeability, as well as the degree of opening and closure dynamics, facilitated by passive cavitation detection and cavitation-guided imaging (31-34).

The Mechanical Index (MI) is often used in diagnostic ultrasonography safety evaluation for non-thermal impacts. Ultrasound systems in the US are limited to an MI of < 1.9; more cautious limitations are recommended in the presence of gas bodies to reduce the danger of cavitation (28,35). MI was developed for brief pulses in liquids; hence, risk evaluation for mechanical bioeffects should be informed by modality-specific exposure context (pulse length, duty cycle, tissue viscoelasticity, and contrast agent usage)(22, 27).

Thermal effects

Ultrasound thermal effects arise when acoustic energy is absorbed in tissue and converted to heat, producing a spectrum of clinically useful phenomena from mild hyperthermia (therapeutic warming) through controlled coagulative necrosis (thermal ablation); the local rate of energy deposition, the resulting temperature rise, and the duration of heating determine the distinction between these endpoints. In ablative applications such as HIFU, acoustic focusing produces very high focal intensities that raise tissue temperatures in the focal zone rapidly (typically reaching >55 ˚C within seconds) and induce irreversible protein coagulation and cell death by coagulative necrosis; this focal mechanism underlies the clinical use of HIFU for tumor and fibroid ablation (36). Thermal modeling of these processes must account for conductive heat transfer, perfusion-mediated convective cooling, and tissue heterogeneity; the Pennes bioheat formulation and its modern variants remain the practical basis for predicting temperature fields and designing safe sonication protocols, although porous-media and two-phase models are increasingly used to capture perfusion and vaporization effects in highly perfused or ablative regimes (37). Because biological outcome depends on both temperature and exposure time, thermal dose metrics such as cumulative equivalent minutes at 43 ˚C (CEM43) provide a quantitative way to relate different time–temperature histories to expected tissue injury and are commonly used for safety guidance and treatment planning; published threshold ranges (e.g., minutes at given CEM43) help delineate mild, reversible heating from permanent tissue damage (38). Clinically, the thermal domain between ~40-45 ˚C (mild hyperthermia) and the ablative range

(>55 ˚C) is exploited for different therapeutic aims: mild hyperthermia is used to increase tumor perfusion and vascular permeability, sensitize tissue to radiation, and trigger thermally responsive drug carriers, while ablative heating is intended to produce immediate coagulative necrosis of the target. Focused ultrasound platforms (including MR-guided HIFU) permit spatially selective application of both sustained mild hyperthermia and short high-temperature ablation with real-time thermometry and feedback control, enabling local activation of thermosensitive liposomes or other thermal release systems for on-demand drug delivery (39). Mechanistically, thermal bioeffects are multifactorial: at the molecular level heat induces protein unfolding and aggregation, denaturation of structural and enzymatic proteins, disruption of lipid membranes and ion channel behavior, and mitochondrial dysfunction; at the cellular level these molecular insults lead to loss of membrane integrity, impaired ATP production, and activation of regulated death pathways (apoptosis, necrosis, or necroptosis depending on dose and context). Significantly, sub-ablative hyperthermia (≈39-43 ˚C) can transiently increase blood flow, oxygenation, and endothelial permeability effects that enhance drug and nanoparticle delivery and increase radiosensitivity by reducing hypoxia. In contrast, ablative heating causes immediate cell necrosis and a local sterile inflammatory response that can alter immune cell recruitment and antigen presentation (40). From a translational perspective several practical considerations follow: precise dosimetry and thermometry are essential to confine therapeutic heating and protect adjacent structures (skin, nerves, vascular walls), and CEM43-based or Arrhenius-based damage predictions must be validated for each tissue type and sonication regime; treatment planners must also consider perfusion heterogeneity (which alters cooling), tissue acoustic properties (which determine absorption and focusing), and the potential for cavitational heating or mechanical damage at high intensities. Real-time imaging (MRI thermometry or ultrasound thermometry, when feasible), robust feedback control of power and duty cycle, and validated treatment planning models are therefore central to the safe clinical deployment. Finally, the overlap between thermal therapies and immunology, whereby ablation-released antigens and hyperthermia-induced stress signals can both prime or suppress immune responses depending on parameters, presents both opportunity and risk: combined thermal+immunotherapy strategies require careful optimization of temperature, timing, and fractionation to harness immunogenic cell death while avoiding excessive tissue injury or counterproductive immune suppression. The revised section thus frames ultrasound thermal effects not as a single mechanism but as a controllable continuum whose clinical utility depends on accurate biophysical modeling, validated dosimetry, and careful integration with drug/radiosensitizer design and immune-modulatory strategies (36).

Sonochemical effects

Nanoparticles known as "ultrasound-responsive nanozymes" are designed to replicate the catalytic activities of natural enzymes while providing the exceptional capacity to be altered by acoustic waves. Their structure or functional state may be altered by ultrasound exposure, enabling highly accurate, on-demand modulation of catalytic activity (41). These nanozymes have great potential for a range of biological applications, including therapeutic interventions, targeted drug delivery, and diagnostic imaging. They are beneficial in nanomedicine because of their ability to have catalytic activity remotely controlled by non-invasive ultrasonography. When triggered by external stimuli, nanosystems with dual redox pairs, such as Fe^{2+}/Fe^{3+} and Cu^{+}/Cu^{2+}, are particularly good at producing hydroxyl radicals (·OH) via Fenton or Fenton-like reactions. Ultrasound has been effectively used in cancer treatment to improve sonodynamic therapy (SDT) and allow regulated chemotherapeutic medication delivery. Ultrasound creates cavitation bubbles that burst and produce strong localized vibrations by generating concentrated shock waves. The diffusion of nanozymes is enhanced by this sonic cavitation mechanism, which significantly speeds up Fenton and Fenton-like reaction rates and increases therapeutic effectiveness (42). Thus, photothermally and US-enhanced CDT may be appropriately integrated onto a nanozyme to effectively prevent tumor growth and recurrence (43-45). Numerous nanozyme formulations have been developed and are still under study; they all exhibit excellent bioactivity and distinct behaviors upon exposure to ultrasonic radiation. In a relevant biological context, it is well established that oxidative stress-induced osteoblast dysfunction is a central pathogenic factor in the development and progression of osteoporosis, affecting the ability to form new bone and remodel existing bone (46). MC3T3-E1 cells were used to create an H_2O_2-induced oxidative stress model to determine if TOPH-200 might reduce oxidative damage in osteoblasts. Following a 24-hour incubation period, cytotoxicity tests revealed that TOPH-200 was non-toxic at doses ranging from 0 to 500 μg/ml. Furthermore, TOPH-200 stimulated osteoblastic proliferation in a dose-dependent manner throughout the 0-125 μg/ml range. These results led to the selection of moderate doses of 5, 25, and 125 μg/ml for further investigations (43). Cell viability decreased to 50.78% in the H_2O_2-treated model group in comparison to the blank control. At dosages of 5, 25, and 125 μg/ml, TOPH-200 treatment increased survival rates to 55.15%, 61.87%, and 65.72%, respectively, restoring viability in a dose-dependent manner. Comparing TOPH-200 to the model group, fluorescence intensity decreased by 12.85% (5 μg/ml), 32.27% (25 μg/ml), and 45.35% (125 μg/ml) in a dose-dependent manner, lowering H_2O_2-induced intracellular ROS levels in MC3T3-E1 cells. Since mitochondrial membrane potential (MMP) is essential for maintaining cellular redox equilibrium, decreases in MMP are well recognized as a significant indicator of cellular health issues (47). TOPH-200 also reversed the H_2O_2-induced decrease in MMP by 12.94%, 58.59%, and 76.70% at doses of 5, 25, and 125 μg/ml, respectively, compared with the model group, in keeping with the ROS results. All of these findings show that TOPH-200 effectively reduces oxidative stress induced by $H2O_2$ and protects osteoblastic MC3T3-E1 cells from mitochondrial damage.

Structural & functional alterations

Microbubbles (MBs) and ultrasound hold considerable promise for enhancing medical delivery. When ultrasonic waves stimulate MBs, they cavitate and exhibit oscillatory bubbles. The encapsulated medication may be released when focused ultrasonography causes it to burst. Drug release and cell membrane permeabilization may happen

simultaneously when drug-loaded MBs are insonated. Additionally, MBs can be visualized in real time using low-intensity ultrasonography, enabling monitoring and guiding the delivery process (48, 49). Additionally, by using ultrasound-triggered microbubble destruction, MBs can be combined with other nanocarriers to enhance targeted drug delivery (50-52).

The cell membrane is a dynamic and adjustable interface for better drug administration, as shown by recent developments in ultrasound-mediated tumor treatment. One prominent example is the use of nanobubble–liposome conjugates, which improve the intracellular absorption of therapeutic drugs by facilitating deep-tissue penetration via ultrasound-triggered membrane permeabilization (53). Likewise, ultrasonic-responsive nanogels have been created to change the permeability of membranes and deliver chemotherapeutic payloads straight into tumor cells, all the while altering the tumor microenvironment to enhance treatment results (54). Nanoscale carriers may provide better tumor membrane engagement and drug delivery efficiency when activated by ultrasound, as evidenced by stronger membrane interactions and higher intracellular drug accumulation in orthotopic liver tumor models compared with microbubbles (55). These findings collectively indicate a trend toward the development of ultrasound-responsive technologies that actively interact with the membrane to deliver effective, spatially regulated therapeutic administration.

DNA damage is a significant factor in the development of many human illnesses, including cancer, according to an earlier study. Cells are constantly subjected to internal and external substances that may cause flaws in either one or both DNA strands (double-strand breaks, or DSB) or just one strand (single-strand breaks, or SSB). Genetically encoded molecular processes repair this damage by removing damaged DNA segments via nucleotide excision repair (NER) or correcting misplaced nitrogenous bases via base excision repair (BER). Even in apparently healthy cells, programmed cell death may occur when the cell is unable to repair its genetic integrity completely (56, 57). It was shown many years ago that the US could alter the structure of DNA. Until recently, it was thought that sonoporation-mediated modifications to genomic DNA involve chemical and mechanical processes (58, 59). Additionally, mechanical stimuli resulting from exposure to the United States may be transduced and activate appropriate effector mechanisms, which, in turn, alter gene expression (60-62).

The most common kind of DNA damage is single-strand breaks (SSBs), which may be caused directly by reactive oxygen species (ROS) or indirectly by enzyme activities during BER. In 1977, McKee and associates noticed strand breaks in DNA solutions subjected to ultrasonic degradation (UD), providing the first proof of SSBs caused by ultrasound. They explained this action by claiming that the sonolysis of water molecules produced free radicals (63). In 1986, Pinamonti *et al.* (64) showed that Sonoporated human leukocytes also contain SSBs. Later research showed that the primary cause of these disruptions is intracellular ROS formation. At the same time, external free radicals had no discernible effect on SSB levels, most likely because of their very short half-lives and incapacity to enter the cell nucleus (65-67).

Since the lack of an unbroken template strand requires the cell to repair the lesion in a predominantly random fashion, double-strand breaks (DSBs) are the most severe kind of DNA damage. Kondo and colleagues published the first known report of ultrasound-induced DSBs in 1985 (68). Later, a neutral comet test was used to validate them in other leukemia cell lines (56). Interestingly, the molecular signaling pathways triggered by ionizing radiation (IR) and by sonoporation-induced DSBs differ. Histone H2AX is phosphorylated at serine 139 (γH2AX) upon DSB occurrence, forming a scaffold for the recruitment of repair-related DNA damage response proteins. Members of the phosphatidylinositol 3-kinase–related kinase (PIKK) family, which includes ataxia-telangiectasia and Rad3-related protein (ATR), DNA-dependent protein kinase (DNA-PK), and ataxia-telangiectasia mutant (ATM), facilitate this phosphorylation. Thus, γH2AX is a known biological indicator of DSBs, and sonoporated cells have been shown to exhibit it (56). IR or medications often activate ATM, and replication stress does so as well (69-71). ATM binds to the MRE11/RAD50/NBS1 (MRN) complex, which helps in homologous recombination (HR) and DSB detection. The Ku70/Ku80 heterodimer, which stabilizes DNA ends and facilitates repair via the non-homologous end-joining (NHEJ) pathway, is also recruited in conjunction with DNA-PK. In sonoporated cells, ATM, DNA-PK, and NBS1 activation have all been experimentally verified (72, 73). According to recent research, sonoporation appears to activate DNA-PK more selectively than ATM. In particular, DNA-PK was shown to be phosphorylated at serine 2056 (pS2056-DNA-PK) on the periphery of nuclei, where it colocalized with γH2AX. On the other hand, phosphorylation of serine 2609 happened without the involvement of γH2AX. According to these findings, pS2056-DNA-PK has two functions: it stimulates DNA damage signaling by activating H2AX and facilitates NHEJ repair of ultrasound-induced DSBs. In addition to its mechanical effects, the kinetic energy of ultrasound may damage DNA by denaturing proteins bound to DNA and promoting the production of reactive oxygen species. However, it has been shown that heat stress preferentially activates ATM over ATR or DNA-PK. Abdollahi *et al.* shed light on this matter by contrasting the effectiveness of sonoporation in lymphoblasts with and without the p53 gene. Both p53-positive and p53-deficient cells were shown to be efficiently killed by ultrasound, while the latter showed more resistance to the activation of apoptosis (74). Additionally, Furusawa *et al.* demonstrated that ATM activity mediates the phosphorylation of p53 at serine 15, and that apoptosis was only inhibited in p53-positive cells when ATM was inhibited (75).

On the other hand, it was discovered that DNA-PK controls Akt phosphorylation and that inhibiting DNA-PK decreased the cell death caused by sonoporation in both p53-positive and p53-negative cells. The authors hypothesized that DNA-PK would be a viable molecular target for ultrasound-based anticancer treatments, based on these findings (75). Consistent with all the data shown, cells exposed to the US had much longer DNA replication, up to 250%, indicating considerable DNA damage (76). According to Hassan and colleagues, sonoporation may promote necrotic division as a survival tactic to increase tolerance to detrimental physiological or environmental stimuli and extend cellular longevity, especially in p53-mutated cells (77).

Cell-type-specific responses

The extracellular matrix, a variety of immunological and stromal populations (including endothelial cells), tumor cells, and soluble factors, including growth hormones and cytokines, comprise the highly dynamic tumor microenvironment (TME)(78).

Tumor vs. normal cells

Fibroblasts and other stromal cells are examples of nearby normal cells that tumor cells aggressively rewire into pro-tumorigenic traits. Unlike their healthy counterparts, these stromal cells contribute to angiogenesis, promote tumor invasion, and create an immunosuppressive environment when transformed (79, 80).

Immune cells

Immune cell populations are often skewed toward immunosuppressive phenotypes by the TME. This environment usually recruits or induces regulatory T cells (Tregs), myeloid-derived suppressor cells (MDSCs), and M2-polarized macrophages, which inhibit anti-tumor immune responses and encourage tumor development and spread (81, 82).

Endothelial cells (ECs)

Normal endothelial cells and tumor endothelial cells (TECs) exhibit distinct phenotypes and functions. Through mechanisms including endothelial anergy, in which decreased expression of adhesion molecules restricts immune cell attachment and transendothelial migration, they promote aberrant angiogenesis and impede immune cell infiltration (78). TECs are both immune response modulators and barriers, as they may present antigens, affect T cell function, and form tertiary lymphoid structures (Table 1)(78, 83).

Translational research applications

Drug & gene delivery

Sonoporation, the temporary permeabilization of cell membranes caused by ultrasound in the presence of microbubbles, has emerged as a potent and adaptable non-viral method for site-specific medication and gene delivery. Microbubble-assisted ultrasound enables targeted, enhanced *in vivo* transfection with plasmid DNA (pDNA). Strong luciferase expression was observed in the rat knee synovium following intra-articular injection of pDNA with microbubbles and ultrasonic exposure, as reported in a noteworthy study. Co-delivering siRNA in the same setting achieved efficient, localized gene suppression (109). Sonoporation has shown promise for delivering siRNA into difficult-to-transfect immune cells, as well as into rapidly growing cell lines. Yamaguchi *et al.* showed that siRNA transfection in freshly isolated primary human and mouse T cells was enhanced by microbubble-assisted ultrasound, resulting in a significant reduction in target protein expression while maintaining high cell viability (110). Sonoporation has recently been expanded to include genome editing using CRISPR/Cas9. Cas9/sgRNA ribonucleoprotein (RNP) and a sonosensitizer were co-encapsulated in an ultrasound-responsive nanosystem created by Wu *et al.* Reactive oxygen species produced by the system's ultrasonic activation disrupted lysosomal membranes, allowing the Cas9 RNP to enter the cytosol and then the nucleus. This method produced effective gene editing in models of hepatocellular cancer (111, 112). When taken as a whole, these results highlight sonoporation's great translational potential for targeted gene therapy and genome editing by demonstrating its ability to deliver a variety of nucleic acid cargos, such as pDNA, siRNA, and CRISPR/Cas9, with precise spatial targeting, low invasiveness, and a favorable safety profile in comparison to viral vectors.

Table 1. Ultrasound effects on tumor microenvironment components, implications, and associated risks

Cell Type/Context	Description in TME	Ultrasound-Relevant Implications	Challenges / Risks	References
Tumor cells	To promote angiogenesis, invasion, and immunosuppression, malignant cells control fibroblasts and stromal cells	Ultrasound may boost therapeutic payload penetration, improve drug delivery, and promote membrane permeability	Risk of encouraging the survival or growth of tumor cells if ultrasonography conditions cause sub-lethal stress	(84-86)
Normal stromal cells	Preserve tissue homeostasis, but tumor signals can convert them into a pro-tumor phenotype	US-triggered cavitation may transiently disrupt tumor–stromal signaling and restore anti-tumor function	Targeting just tumor-altered stromal cells while avoiding harming healthy tissue is challenging	(86-88)
Regulatory T cells (Tregs)	Suppress the activity of effector T cells that are high in TME	Low-intensity US may increase anti-tumor immunity or alter Treg recruitment	Autoimmunity may result from off-target immune activity	(89-91)
Myeloid-derived suppressor cells (MDSCs)	Suppress T cell responses and promote tumor development	US-induced ROS and mechanical forces may locally reduce MDSC numbers and functions	Overproduction of ROS may damage healthy immune cells	(92-95)
M2-polarized macrophages	Characteristics that promote angiogenesis and are pro-tumoral	Ultrasound may restore anti-tumor effects by reprogramming the M2 to M1 phenotype	After therapy, maintaining the long-term M1 phenotype is still difficult	(96, 97)
Tumor endothelial cells (TECs)	Low expression of adhesion molecules ("endothelial anergy"); abnormal, leaky vasculature	Ultrasound may promote immune cell infiltration and temporarily enhance TEC permeability	Uncontrolled cavitation increases the risk of vascular rupture or bleeding	(98, 99)
Normal endothelial cells (ECs)	Control the immune system and proper vascular permeability	More resilient than TECs to permeability changes brought on by the US	Has to be precisely targeted in order to prevent damaging healthy vasculature	(100, 101)
TECs as immune modulators	Antigen presentation, T cell activation regulation, and tertiary lymphoid structure formation	The US may improve the ability to present antigens	If the presentation is unbalanced, there is a risk of inducing undesired immunological tolerance	(102–104)
Extracellular matrix (ECM)	Dense, aberrant network that limits medication and immunological penetration	To improve treatment administration, Ultrasound may temporarily alter the density of the extracellular matrix	By releasing tumor cells, excessive disruption may encourage spread	(105, 106)
Soluble factors (cytokines, growth factors)	Control the activation, differentiation, and recruitment of immune cells	US may modify immune migration by changing cytokine gradients	Possible induction, under some circumstances, of pro-tumor cytokine profiles	(107, 108)

Microbubbles and ultrasound-responsive nanocarriers have evolved into powerful vehicles for targeted gene and drug delivery, enabling precise temporal and spatial control of therapeutic release. They use mechanical and physical processes induced by ultrasound, including cavitation, acoustic streaming, and localized heating, to temporarily increase vascular permeability and enhance the uptake of therapeutic substances by cells (113, 114).

When subjected to ultrasound, microbubbles, which typically consist of a gas core surrounded by a lipid, polymer, or protein shell, oscillate (Figure 2). While inertial cavitation may break vesicles and enhance intracellular transport at higher pressures, stable cavitation occurs at moderate acoustic pressures, temporarily boosting cell membrane permeability (115). In addition to serving as delivery vehicles, microbubbles may enhance site specificity by conjugating with medicines, nucleic acids, or targeting ligands.

Liposomes, polymeric nanoparticles, micelles, and phase-change nanodroplets are examples of ultrasonically responsive nanocarriers designed to release their cargo in response to ultrasound stimulation. Thermosensitive liposomes loaded with doxorubicin, for instance, have shown selective drug release at sonicated tumor locations, increasing intratumoral drug levels while reducing systemic toxicity (116). Likewise, acoustic droplet vaporization of perfluorocarbon nanodroplets may produce microbubbles in situ, enabling the combination of triggered treatment and imaging (117).

The integration of diagnostics (ultrasound imaging) and therapy (drug or gene delivery) into a unified "Theranostic" platform greatly amplifies the clinical value of these systems. By enabling precise, minimally invasive, and image-guided interventions, ultrasound-responsive nanocarriers and microbubbles offer strong potential for applications such as targeted cancer treatment, thrombolysis, and localized gene transfection.

Molecular imaging

Ultrasound

Because ultrasound molecular imaging can provide quick, safe, and noninvasive results, all of which are essential for AR, it is increasingly respected (118, 119). The promise of targeted ultrasonography in transplant monitoring was shown by Weller *et al.*, who were the first to visualize intragraft T cells and intercellular adhesion molecule-1 (ICAM-1) expression using this modality (120). In a similar vein, Jin *et al.* evaluated acute rejection in a mouse heart transplant model using manufactured microbubbles loaded with either anti-granzyme B antibodies (MBGzb) or isotype control antibodies (MBcon)(121). Myocardial contrast signals in the allogeneic MBGzb group decreased precipitously, and a few seconds after the flash pulse, the microbubbles gradually recovered. In comparison to the allogeneic and syngeneic MBcon groups, this group also showed a significantly higher decrease in peak intensity on postoperative days 2 and 5. Granzyme B (GzB) expression may be dynamically and reliably quantified *in vivo* using this technique, providing a valuable indicator for tracking rejection reactions. Nevertheless, signal loss due to microbubble disintegration may compromise the precision of these observations (122).

Antibody-mediated rejection (AMR) after heart

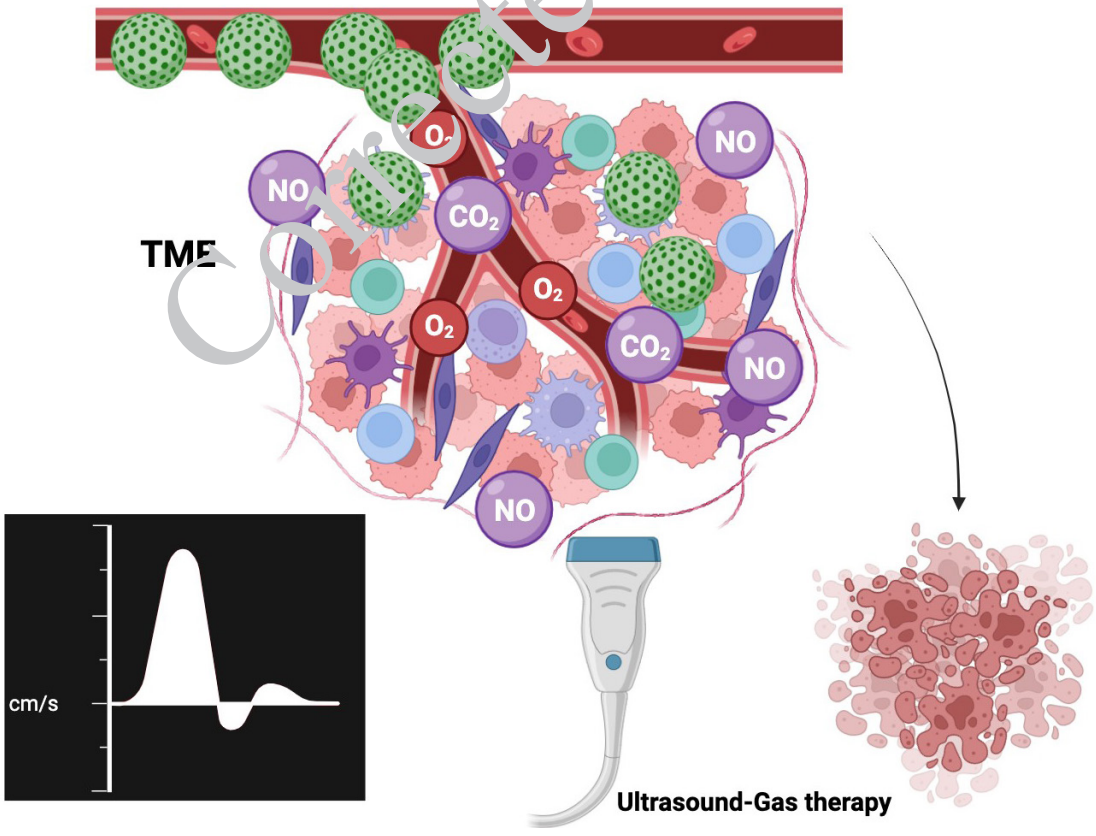

Figure 2. Schematic overview of ultrasound-triggered gas therapy
Ultrasound exposure induces the release of therapeutic gases such as NO, O_2, CO, and CO_2 from gas-releasing molecules for tumor treatment

transplantation may now be diagnosed noninvasively because of recent advancements in ultrasonographic molecular imaging. To target and identify acute rejection in heart transplant animals, Liu *et al.* created nanobubbles functionalized with CD3 antibodies (NBCD3)(123). Nanobubble signal intensity increased proportionally with concentration and showed excellent stability, as observed in *ex vivo* imaging. Interestingly, nanobubbles coated with anti-CD3 antibodies showed improved adherence to T cells and increased imaging signals, particularly in allograft-affected rats, indicating increased T lymphocyte infiltration. Although further research is required to confirm its clinical application, this method has significant promise for noninvasive rejection monitoring (124, 125).

Liao *et al.* investigated the quantitative evaluation of rejection levels after heart transplantation using targeted ultrasound imaging and C4d, a particular biomarker for AMR (126). The need for an invasive biopsy has limited the use of C4d, despite its crucial role as a biomarker recommended for AMR monitoring. To overcome this, streptavidin–biotin conjugation was used to create C4d-targeted microbubbles (MBC4d), which were then evaluated in rat heart transplantation models. Targeted ultrasonography demonstrated high sensitivity, enabling real-time visualization of C4d distribution and revealing significant protein expression during AMR episodes. Crucially, MBC4d's safety profile was confirmed by the absence of reduced survival or additional tissue damage upon administration. Given the widespread clinical use of contrast-enhanced ultrasonography, there is a good chance that this noninvasive, safe, and quantifiable method will be quickly included in AMR assessment procedures (127).

Ultrasound molecular imaging is a valuable method for detecting transplant rejection since it allows for continuous, real-time monitoring. Targeted microbubbles are used to assess allograft rejection with high sensitivity by detecting key biomarkers, such as GzB and C4d. However, there are still certain restrictions. In addition to ultrasound's inherently inferior contrast resolution compared with computed tomography (CT) and magnetic resonance imaging (MRI), the physical destruction of microbubbles may impair imaging accuracy. These limitations suggest that ultrasonic molecular imaging would be most effective when combined with other imaging modalities as part of a multimodal diagnostic approach to enhance overall accuracy.

MRI

MRI is a powerful imaging method known for its ability to provide finely detailed anatomical images with superior tissue contrast and high resolution (118, 128). It improves imaging quality by using T1 and T2 contrast agents, which makes it very helpful for tracking transplant rejection and looking at different biochemical processes (129). Recent studies in immune cell-based molecular imaging have highlighted MRI's capacity to provide comprehensive insights into the processes of immune-mediated rejection. It is beneficial for the early diagnosis of acute cellular rejection (ACR) due to its high sensitivity in monitoring immune cell trafficking and function. In a rat heart transplantation model, Guo *et al.* effectively introduced pDNA and superparamagnetic iron oxide nanoparticles (SPIO) into primary T cells (130). SPIOs conjugated to a CD3 single-chain antibody/pDNA polymer were used to accomplish this (131). Guo *et al.*'s delivery method consisted of superparamagnetic iron oxide nanoparticles (SPIONs) and PEG-g-PEI functionalized with a CD3 single-chain antibody (scAbD3). On MRI-balanced turbo field echo pictures of the transplanted hearts, rats given targeted polyplexes harboring a null plasmid showed clear low-signal patches between days 0 and 10 post-transplantation, suggesting targeted polymer buildup in the allografts. Effective gene transfection in T cells was also made possible by this platform, and gene therapy dramatically reduced the immunological response in transplanted rats. All things considered, this approach provided real-time feedback on treatment effectiveness while enabling noninvasive MRI monitoring of the entire therapeutic process.

Macrophages are great candidates for noninvasive *in vivo* immune cell imaging because of their inherent ability to phagocyte contrast agents and their ease of labeling in situ with iron oxide particles. Wu *et al.* demonstrated this by visualizing macrophages and detecting organ rejection *in vivo* using cellular MRI with iron oxide particles (131, 132). Macrophages were chosen as targets because of their essential role in autoimmune disorders, inflammation, and organ rejection (133, 134). Additionally, it has been shown that T cells and lymphocytes may be tracked by MRI (135 ,136). Liu *et al.* modified SPIO nanoparticles with amination to increase T cell absorption of the particles (136). Using EDAC-coupling processes, the researchers created IOPC-NH_2 particles from IOPC cores. T cells were labeled, reinfused, and then aggregated in allogeneic lung and heart transplants, allowing for the early MRI identification of transplant rejection. When immune cells absorb tiny SPIO particles, they become magnetically sensitive and may clump together in inflammatory regions, making them visible on MRI. These tagged immune cells demonstrated strong adherence to target tissues and high biosafety. Specialized contrast agents, such as SPIOs, are used in MRI molecular imaging to track cellular and pathological alterations, particularly when combined with immune cell targeting. High spatial resolution and excellent soft-tissue contrast are two significant benefits of this method, making it ideal for in-depth immune surveillance in transplantation settings (137). However, several challenges remain in the way of this approach's clinical application. MRI often requires greater probe concentrations than other molecular imaging techniques, which might create toxicity issues.

Furthermore, certain patient groups may not be able to obtain an MRI due to its higher cost and longer scan time. However, recent advancements in hyperpolarization techniques and high-contrast probe design have greatly enhanced the capacity to identify biological targets at lower concentrations. With significant significance for the early diagnosis of ACR, these developments are crucial for improving transplant rejection monitoring.

Nuclear medicine imaging

With the use of radioactive tracers for comprehensive imaging, nuclear medicine imaging techniques, most notably SPECT and PET, have emerged as alternative tools for noninvasive monitoring of organ transplant rejection (138). With several successful examples in preclinical models, SPECT has shown significant value in monitoring immune responses after transplantation. Using ^{68}Ga-

labeled CD163 and optically labeled CD206 for targeted macrophage imaging, for example, has validated the viability and efficacy of these molecular imaging techniques (139, 140). To visualize Sn-expressing macrophages, an anti-sialoadhesin (Sn; also known as Siglec-1 or CD169) monoclonal antibody (SER-4) radiolabeled with 99mTc-pertechnetate was used. This method enabled effective monitoring of macrophage infiltration, allowing for the detection of transplant rejection reactions (96, 141).

By measuring T-cell infiltration, SPECT imaging can also be used to track the progression of transplant rejection. A new radiolabeled probe, 99mTc-HYNIC-mAbCD4, was developed by Li *et al.* to identify and track $CD4^+$ T cell infiltration in cardiac transplants (142). Transplanted hearts in allograft patients showed significant radiotracer accumulation within 1 hour of ^{99}mTc-HYNIC-mAbCD4 injection, peaking at 6 hrs. Allograft uptake levels were much greater than those of the autograft and treatment controls. The potential of SPECT/CT imaging for noninvasive monitoring and diagnosis of acute cardiac rejection is highlighted by its capacity to distinguish allografts based on enhanced ^{99}mTc-HYNIC-mAbCD4 uptake. Furthermore, Sharif-Paghaleh *et al.* used ^{99}mTc-rCR2 to effectively target the complement component C3, with confirmation from autoradiography and histology. This highlights the potential of SPECT/CT as a robust tool for evaluating transplant-related damage (143).

Another cutting-edge medical diagnostic technique is PET imaging, which is essential for identifying early signs of ACR in transplant recipients (144-148). Two radiotracers were used to assess PET imaging in a prominent murine cardiac rejection model: ^{18}F-fluorodeoxyglucose ($[^{18}F]$-FDG) and ^{13}N-ammonia ($[^{13}N]$-NH_3). Serial $[^{18}F]$-FDG PET imaging showed a significant rise in radiotracer uptake in allografts, particularly between days 14 and 28 post-transplant, which was strongly associated with increasing rejection grades in heterotopic heart transplants with minimal MHC mismatches. In contrast, allografts with chronic vasculopathy showed considerably lower myocardial perfusion on $[13N]$-NH_3 PET imaging than controls. With encouraging implications for clinical translation, our findings together highlight the benefits of combining $[^{18}F]$-FDG with $[^{13}N]$-NH_3 PET imaging for noninvasive, quantitative evaluation of allograft rejection. Building on these developments, the creation of PET probes targeting specific immune cell markers has begun. For instance, Ueno *et al.* employed a novel PET-CT technique to image macrophage activity in allografts, aiming to detect cardiac transplant rejection (149, 150). Similarly, Hirai *et al.* developed an immune PET tracer targeting the OX40 receptor after identifying OX40 as an imaging target for activated T cells (151-153). The temporal dynamics of activated T cell growth and infiltration may be quantitatively assessed using OX40 ImmunoPET, which is in line with flow cytometry findings. Since activated CD4 T cells are the cells that express OX40 the most, ^{89}Zr-OX40mAb was able to identify these cells in transplanted hearts in the early stages of rejection. These results suggest that nanoparticle-enhanced macrophage PET-CT may become a prediction tool for graft survival in addition to offering sensitive identification of heart transplant rejection. Numerous imaging agents in nuclear medicine have previously undergone thorough safety testing and clinical use, especially in cancer. Comparing nuclear medicine imaging to many other molecular imaging techniques, it is hence further down the route to clinical translation for transplant rejection monitoring. This is corroborated by a single-center research by Dar *et al.* that evaluated cardiac transplant rejection using $[^{18}F]$FDG PET-CT, showing that PET may be helpful in early clinical practice for rejection diagnosis (154). Despite persistent worries about the expense and security of PET and SPECT (155). One of the first molecular imaging techniques to be widely used in clinical settings for regular monitoring of allograft rejection is nuclear medicine. More generally, the toolset for rejection monitoring is growing as molecular imaging advances rapidly. Future research will concentrate on developing more intelligent tracers and identifying more valuable biological targets to enable safer, more accurate, and more efficient post-transplant care (Table 2).

While nuclear medicine imaging (SPECT and PET) offers unmatched molecular sensitivity and quantitative capability, its limitations in spatial resolution, radiation exposure, and infrastructure requirements necessitate a balanced evaluation relative to MRI and ultrasound. Unlike ultrasound, which provides real-time, radiation-free imaging, or MRI, which offers high spatial resolution and soft-tissue contrast, nuclear medicine excels at early

Table 2. Molecular imaging modalities for transplant rejection: Principles, targets, benefits, challenges

Modality	Principle / Mechanism	Biomarkers / Targets	Key Benefits	Limitations / Challenges	Key References
Ultrasound molecular imaging (Targeted microbubbles / nanobubbles)	Target molecules are bound by microbubbles or nanobubbles coupled with ligands or antibodies; their number and location are detected by ultrasonic contrast agents	Granzyme B (GzB), CD3 (T cells), C4d (AMR biomarker)	High molecular specificity; noninvasive, reproducible, and real-time; potential for quick bedside use	Accuracy may be lowered by microbubble destruction; contrast resolution is poorer than with CT/MRI; and depth penetration is limited	(156-158)
MRI molecular imaging (SPIO-labeled immune cells / targeted nanoparticles)	T1/T2 MRI signal alterations are produced by immune cells (such as T cells and macrophages) tagged with SPIO or targeted nanoparticles; these cells may combine delivery and tracking	CD3 T cells, lymphocytes, and macrophages	Excellent soft tissue contrast, high spatial resolution, concurrent functional and anatomical imaging, and the ability to monitor immune cell infiltration	Requires high concentrations of the probe, may be harmful to nanoparticles, requires longer scan periods, and is more expensive	(159, 160)
Nuclear medicine imaging (SPECT / PET)	SPECT/PET measures uptake and distribution of radiolabeled antibodies, ligands, or tracers that target immune cells or metabolic processes	$CD4^+$ T cells, complement C3, OX40 (activated T cells), macrophage markers (CD163, CD206, and CD169), glucose metabolism ([18F] FDG), and perfusion ([13N] NH_3)	Extremely sensitive, quantitative, capable of identifying rejection early, and with a well-established clinical infrastructure	High expense, limited tracer supply, radiation exposure, and the potential need for multimodal correlation to achieve specificity	(161-163)

detection of molecular events, such as immune cell infiltration and metabolic changes that precede structural damage. Importantly, its theranostic role is increasingly recognized: diagnostic tracers (e.g., ^68Ga-labeled ligands) can be paired with therapeutic radionuclides (e.g., ^177Lu or ^225Ac conjugates) to achieve a true "image-and-treat" paradigm. This integration places nuclear medicine at the forefront of precision theranostics, particularly when combined with complementary modalities to overcome its individual shortcomings.

Immunomodulation

Ultrasound combined with microbubbles or nanoparticle carriers

By converting "cold" tumors into "hot" ones that are more vulnerable to immune attack, ultrasound offers a unique way to enhance immune responses, particularly when combined with microbubbles or nanoparticle carriers. Ultrasound-targeted microbubble destruction (UTMD), which stimulates many immune-boosting pathways, is a significant cause of this shift (164) Tumor-associated antigens (TAAs) are released when mechanical pressures applied by pulsed or high-intensity focused ultrasound (pFUS/HIFU) momentarily enhance the permeability of endothelial and tumor cell membranes, disrupt stromal structure, and induce targeted vascular damage (165) and molecular patterns linked to damage (DAMPs)(166) such as calreticulin, ATP, and HMGB1, which are essential for the activation of dendritic cells (DCs) and the presentation of tumor antigens to T lymphocytes (167-169).

Second, ultrasound reprograms the cytokine and chemokine profile of the TME. According to studies, pro-inflammatory mediators such as IL-1β, TNF-α, and IFN-γ are rising, while immunosuppressive signals such as TGF-β are falling (170-172).

Third, ultrasound-induced vascular modulation promotes immune cell trafficking and drug delivery to tumor sites by increasing vascular permeability and perfusion (168, 173, 174). Additionally, ultrasound may cause acoustic cavitation and moderate hyperthermia, which increase heat-shock protein levels and enhance antigen cross-presentation, both of which strengthen adaptive immunity. Preclinical research repeatedly shows that, in comparison to untreated tumors, ultrasound-treated tumors had higher activated $CD8^+$ T-cell densities, more robust NK cell activity, and improved antigen presentation (168, 169, 175, 176). When considered together, these impacts create a confined, inflammatory milieu that supports immune-mediated tumor removal.

Combination strategies with immune checkpoint inhibitors and cancer vaccines

Ultrasound is an excellent adjunct to immune checkpoint inhibitors (ICIs) and cancer vaccines, especially those that target PD-1 and PD-L1, by releasing tumor antigens, enhancing vascular function, and drawing effector immune cells (177), or CTLA-4, which have transformed cancer treatment; yet, their effectiveness is often restricted to tumors that are already inflamed by T cells. Ultrasound can bridge this gap by priming immune-desert tumors for checkpoint blockade responsiveness (178, 179). Preclinical findings indicate that pFUS combined with anti-PD-1 treatment dramatically increases survival in melanoma and pancreatic cancer models, primarily by reducing Treg numbers and enhancing CD8 T-cell infiltration (180).

This strategy is supported by early clinical results demonstrating that HIFU combined with immunotherapy is safe, less painful, suppresses local tumors, and may increase systemic immune activity in patients with liver metastases (181). Mechanistically, ultrasound may increase PD-L1 expression on tumor cells, in addition to enhancing antigen release, which may open up new targets for ICIs (167).

These processes also hold for cancer vaccines, which need immune cell activation and potent antigen presentation. Dendritic cell (DC) recruitment and ultrasound-induced DAMP release serve as natural adjuvants that boost vaccine-induced immune responses (182). By using acoustically sensitive carriers, such as phase-change nanodroplets or microbubbles, which release antigens locally upon sonication, ultrasound may also facilitate targeted vaccination administration (183, 184). According to animal research, ultrasound-assisted immunization increases and broadens tumor-specific T-cell responses, improving tumor management compared with vaccination alone.

Optimizing ultrasound settings, improving nanocarrier designs, and determining the best sequencing with ICIs or vaccinations will be necessary for future advancements (185). This comprehensive strategy presents the promise of overcoming immune resistance and achieving long-lasting systemic antitumor immunity. A study showed that more potent systemic antitumor immunity and tumor growth suppression were observed following mechanical high-intensity focused ultrasound (M-HIFU) compared with thermal HIFU (T-HIFU). Single-cell RNA sequencing–based molecular characterization of the tumor microenvironment (TME) post-M-HIFU revealed a pronounced repolarization of tumor-associated macrophages (TAMs) toward the immunostimulatory M1 phenotype, in contrast to the TME changes induced by T-HIFU. Furthermore, the concurrent administration of anti–PD-L1 antibodies or depletion of $CD4^+$ T cells—particularly those containing regulatory T cell populations—substantially enhanced T cell–mediated antitumor immunity and suppressed tumor growth at distant, untreated tumor sites in M-HIFU–treated mice compared with M-HIFU monotherapy. In these combination approaches, $CD8^+$ T cells and natural killer (NK) cells emerged as the primary effector cell populations mediating tumor clearance (Figure 3)(186).

Regenerative medicine

Because ultrasound can be administered remotely and non-invasively while producing a variety of biological effects, it has attracted significant interest in therapeutic medicine. Different intensities and frequencies are used in medical practice for both diagnosis and therapy. Significant therapeutic potential has been shown by low-intensity pulsed ultrasound (LIPUS), particularly in supporting bone regeneration and repair (187). Compared to high-intensity ultrasound, which generates a lot of heat that may damage organs, tissues, and cells, it is much safer. Low-intensity pulsed ultrasonography was first used to hasten fracture healing in 1983 (188, 189). Since then, several investigations have demonstrated that LIPUS can alter angiogenesis and other biological processes (190-200), cartilage formation, and bone remodeling (201, 202), which occur during the repair and regeneration of bone flaws (199, 200). LIPUS has also shown promise in reducing delayed fracture union

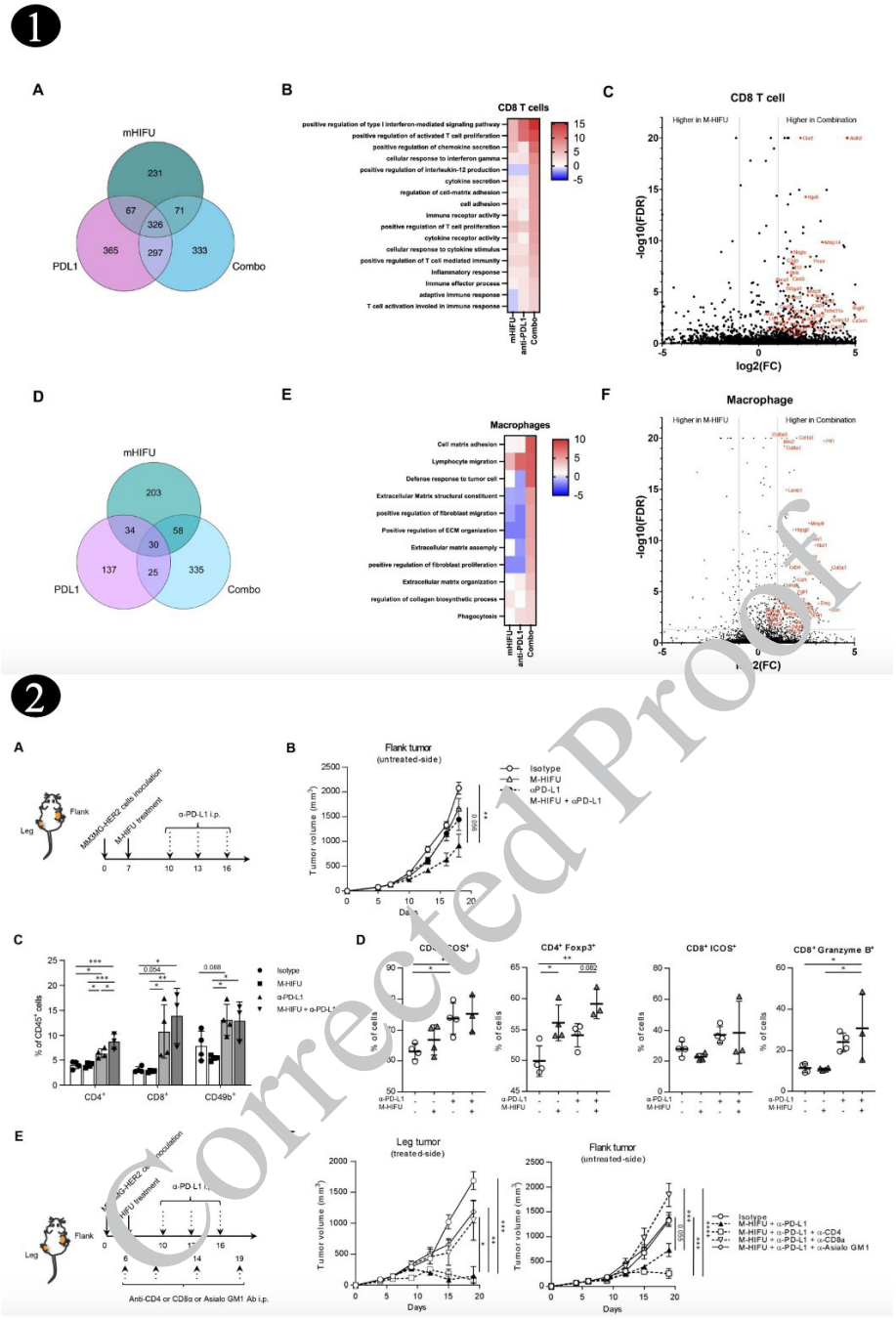

Figure 3. 1) Combination of M-HIFU and anti–PD-L1 antibody modulates unique gene expression in tumor-infiltrating CD8$^+$ T cells and macrophages
MM3MG-HER2 tumors in BALB/c mice were treated with M-HIFU, followed by anti–PD-L1 or control IgG on days 3 and 6. Tumor CD45$^+$ leukocytes were isolated for scRNA-seq. (A, D) Venn diagrams show up-regulated DEGs in CD8$^+$ T cells and macrophages versus controls. (B, E) GO enrichment heatmaps display top-enriched terms for each treatment, with combination therapy highlighted. (C, F) Representative DEGs significantly up-regulated in the combination group compared with M-HIFU monotherapy ($log_2FC>1$, FDR<0.05) are labeled in red, including genes linked to KEGG pathways or M1/M2 signatures
2) Synergistic inhibition of distant tumor growth by M-HIFU and PD-1/PD-L1 blockade depends on CD8$^+$ and NK cells
BALB/c mice bearing MM3MG-HER2 tumors in the leg and flank received M-HIFU to the leg tumor (day 7) and anti–PD-L1 or control IgG (days 10, 13, 16). (A) Experimental design. (B) Growth curves of untreated flank tumors (n=10/group). (C, D) Flow cytometry of immune infiltrates in distant tumors on day 18, showing proportions of CD4$^+$, CD8$^+$, CD49b$^+$ cells, and expression of ICOS, Foxp3, and granzyme B (n=3–4/group). (E) CD4$^+$, CD8$^+$, or NK cell depletion in the same treatment schedule. (F) Growth curves of treated leg tumors (left) and distant flank tumors (right) (n=5/group). Error bars: SE (B, F) and SD (C, D)

in preclinical research over the last several decades (195-197) and in distraction osteogenesis (198, 199), promoting bone defect repair (200, 201) and periodontal tissue regeneration (202). It has also been used in several other models of orthopedic diseases. Usually administered non-invasively via the soft tissue surrounding the bone, LIPUS transforms mechanical impulses into biological ones to aid in the healing process. Both *in vitro* and *in vivo* investigations have shown that ultrasound stimulates many cellular signaling pathways throughout the healing process, indicating the complexity of the molecular processes underlying LIPUS-induced bone regeneration (203, 204). The transformation of mechanical inputs into biochemical signals is facilitated by integrins (205). It has been shown

that interactions with specific protein signaling molecules may convert mechanical inputs into biological signals (206). The phosphorylation of a crucial enzyme known as FAK initiates this process (207). Through integrins, these FAs facilitate the mechanical connection between the intracellular cytoskeleton and the extracellular matrix.

Furthermore, LIPUS may increase RANKL production, which stimulates chondroclasts and osteoclasts, thereby promoting resorption (208). This may aid in the reshaping of bones during the regeneration process. According to research, osteoblastic differentiation increased with longer ultrasonic stimulation time (209). According to a separate study, Piezo1 channels act as a second messenger to initiate ERK1/2 activation and perinuclear F-actin polymerization, which together stimulate cell proliferation by converting mechanical stresses produced by LIPUS into intracellular Ca2+ influx (Table 3)(210).

Safety, challenges, and future directions

Safety standards and regulations

Ultrasound is often regarded as harmless when administered correctly; however, its acoustic energy can cause damage through thermal and mechanical effects. To evaluate and mitigate these hazards, output display standards (ODS) mandate the presentation of two safety metrics, the Thermal Index (TI) and MI on the display screen (29).

Thermal index (TI) and mechanical index (MI) guidelines

The TI predicts the potential increase in tissue temperature approximately 1 ˚C per unit under extreme conditions. It functions as an essential safety precaution; for example, Doppler ultrasound modes often elevate TI. In first-trimester fetal imaging, TI values above 0.7 should be avoided, and values above 3.0 are strongly discouraged. A recent NHS audit of more than 2,600 ultrasound sessions found substantial adherence to TI recommendations, with violations occurring in around 1% of obstetric cases, mainly during pulsed Doppler use (222).

The MI measures the possibility of cavitation and other non-thermal bioeffects. It is calculated by dividing the derated peak rarefactional pressure by the square root of the center frequency. The classical Minnaert equation describes the resonance frequency of a free gas bubble in a liquid:

$$fres = \frac{1}{2\pi R}\sqrt{\frac{3\gamma P0}{\rho}}$$

Where ρ is the density of the surrounding liquid (kg/m^3), P_0 is the ambient static pressure (Pa), γ is the specific heat ratio of the encapsulated gas, and R is the radius of the bubble (m). Smaller bubbles resonate at higher frequencies, while larger bubbles reverberate at lower frequencies, as shown in this connection. Matching the driving frequency to or close to the bubble's resonance in real-world ultrasonic applications optimizes volumetric oscillations. It amplifies mechanical effects like microstreaming and shear stress production, which improve therapeutic effectiveness and diagnostic contrast.

MI is capped at 1.9 in diagnostic circumstances by FDA and AIUM regulatory recommendations; levels below this threshold have not been associated with any negative consequences in tissues devoid of gas bodies (29, 223). Still, non-thermal risks may arise in gas-containing organs, such as the lungs (threshold MI ~0.4) and intestines (MI ~1.4) (29, 223). New consensus standards (such as ITRUSST) for both therapeutic and malignant ultrasonography confirm that keeping TI and MI within acceptable boundaries, and keeping MI < 1.9, maintains thermal increase below 2 ˚C or thermal dosage below 0.25 CEM. 43 safety (29).

Minimizing off-target tissue injury

Although rare, thermal and mechanical hazards from ultrasonography may still occur, especially in delicate tissues, despite stringent regulations. Ultrasound absorption and heating cause thermal injury, which is more severe in tissues with poor blood flow, such as the cornea, lens, bone, and fat. While tissue perfusion and metabolic activity affect heat removal, acoustic intensity, target area, frequency, and exposure length all affect the quantity of heat generated (29).

Table 3. Ultrasound-mediated immunomodulation and regeneration: Mechanisms, applications, benefits, and challenges

Application	Mechanism	Clinical / Preclinical Applications	Benefits	Challenges / Limitations	References
Immunomodulation via Ultrasound	Vascular modulation, the release of TAAs and DAMPs (HMGB1, ATP, calreticulin), mechanical disruption of tumor/stromal cells, and cytokine profile reprogramming toward pro-inflammatory states are all caused by UTMD, pFUS, or HIFU	Transformation of "cold" cancers into "hot" tumors; increased activation of CD8 T cells, NK cells, and DCs	Targeted inflammation, noninvasive immune activation, and possible systemic anti-tumor benefits	Preventing excessive tissue or vascular damage; striking a balance between toxicity and immunological activation	(54, 211-213)
Combination with Immune Checkpoint Inhibitors (ICIs)	Ultrasound enhances tumor responses to PD-1, PD-L1, or CTLA-4 inhibition by augmenting antigen release, PD-L1 expression, and immune infiltration	Synergistic treatment in models of melanoma, pancreatic, and liver metastases; enhanced survival and tumor management	Surmounts immunological resistance; augments the effectiveness of current immune checkpoint inhibitors	Optimal sequencing of immune checkpoint inhibitors is not standardized; there is a risk of immune-related side effects	(172, 214-217)
Combination with Cancer Vaccines	Ultrasound induces the release of TAAs/DAMPs, attracts dendritic cells, and functions as an adjuvant; it may also facilitate the localized release of TAAs/DAMPs from acoustically sensitive carriers	Improved antigen presentation and T-cell activation in tumor models; increased vaccine-mediated tumor suppression	Enhances the scope and intensity of the immunological response; targeted administration is feasible	Demands exact targeting; contingent upon carrier configuration and ultrasonic specifications	(125, 218, 219)
Regenerative Medicine (LIPUS)	Low-intensity pulsed ultrasound converts mechanical energy into biochemical signals via integrins, FAK, Piezo1-mediated Ca^{2+} influx, and ERK1/2 activation, so facilitating angiogenesis, osteogenesis, and cartilage regeneration	Healing of bone fractures, distraction osteogenesis, restoration of bone defects, and regeneration of periodontal tissue	Secure, noninvasive, reproducible; enhances tissue regeneration; regulates several regenerative pathways	Inconsistent effectiveness in clinical trials; limitations in deep penetration; necessitate prolonged treatment durations	(187, 211, 220, 221)

Practitioners should follow the ALARA ("As Low as Reasonably Achievable") principle to minimize exposure time, use the lowest power settings, and carefully adjust the ultrasound focus and mode to reduce risks. This is especially important when using Doppler or pulsed-wave modes, which tend to produce higher thermal effects (224).

According to recent research, doctors seldom actively monitor bioeffect indicators such as the TI and MI, despite their detection during ultrasound tests. For instance, although all scans were within acceptable limits, eye-tracking research showed that operators looked at these safety warnings in only 4% of regular obstetric scans. This shows a severe human factor deficiency in preserving safety consciousness (223-225).

Challenges in translation

The two primary interrelated obstacles to the therapeutic use of ultrasound-responsive drugs are manufacturing/regulatory complexity and patient-related variability. Significant heterogeneity is created by variations in patient anatomy, including tissue composition, depth, and blood artery distribution, which affects how ultrasound waves concentrate, travel, and activate contrast agents. Furthermore, the dependability of ultrasonic dosage delivery and microbubble response is diminished by differences in tissue attenuation and dispersion across various body types and organs (226). Achieving consistent imaging quality and efficient therapeutic administration, such as sonoporation and cavitation-driven drug release, is significantly hampered by this inconsistency (227, 228). To overcome these problems, quantitative ultrasound techniques estimate and adjust for tissue attenuation coefficients in real time (229). Nonlinear tissue responses and the absence of reliable reference data, especially in living systems, allow substantial variability to persist (230). These difficulties are exacerbated by operator variability: portable ultrasound imaging and therapy are not standardized, and variations in probe angle, pressure, and placement occur across operators and between scans performed by the same operator (231). Significant variations in picture quality and therapy efficacy result from this discrepancy (232).

In addition to biological and technological heterogeneity, manufacturing difficulties and regulatory ambiguities impede clinical implementation. Microbubbles and multifunctional nanoparticles are examples of ultrasonically responsive agents that need exact control over parameters, including size distribution, shell composition, payload loading, and ultrasound sensitivity. A thorough evaluation of their physicochemical characteristics, including particle size, structural integrity, and payload retention, as well as long-term storage stability and consistency across manufacturing batches, is necessary to ensure large-scale repeatability (233). Regulatory obstacles are significant: these drugs' dual function as therapeutic and diagnostic instruments (also known as "theranostics") makes it more difficult to classify and evaluate them. Regulatory bodies need thorough preclinical safety (234), information on pharmacokinetics, imaging effectiveness, and treatment performance.

Nevertheless, regulatory regimes often do not provide specific guidance for new stimuli-responsive carriers or nanotheranostics, which increases uncertainty around submission expectations and lengthens the time to market (235, 236). Early innovators sometimes face lengthy regulatory assessment processes; in new device categories, approval delays for first entrants may be several months longer than for subsequent applications. The primary causes of this include ambiguous application criteria, a lack of past instances to serve as a reference, and confusion over submission forms (237).

When combined, these difficulties, variability among patients and operators, and manufacturing and regulatory barriers create a bottleneck for the rapid, reliable, and scalable translation of ultrasound-responsive medicines (238). Innovations in accurate imaging and delivery calibration, automation to reduce operator variability, scalable production with strict quality control, and proactive cooperation with regulatory agencies to provide clear clearance paths are all necessary to overcome these obstacles. Together, these factors must be addressed to transition from laboratory proof-of-concept to a dependable, safe, and successful clinical application (239).

Emerging frontiers

AI-enhanced image interpretation and treatment planning

The use of artificial intelligence (AI) in ultrasonic imaging, such as convolutional neural networks and deep learning, has been shown to significantly increase diagnostic efficiency and accuracy in recent systematic evaluations. Regardless of the operator or clinical setting, these AI strategies have been used to improve lesion identification, picture quality, and consistency in interpretation across 2D, 3D, and Doppler ultrasound modalities (240). Autonomous multimodal large language model (LLM) agents have been developed for targeted ultrasonic ablation in treatment planning (240, 241). For example, consider the FUAS Agents system, which generates customized treatment regimens by integrating MRI data, image segmentation, dosage prediction, and clinical guideline retrieval (241). Expert assessments of the plans' completeness, correctness, fluency, and adherence to guidelines in a research study on uterine fibroids yielded ratings of 82.5% or higher, with clinical compliance at 97.5% (242).

Wearable and implantable ultrasound devices for continuous monitoring or therapy

The creation of intelligent health monitoring systems increasingly relies on AI-enhanced sensors. These sensors provide enhanced functionality and simplicity for applications involving continuous physiological monitoring (243). At the same time, regulated, on-demand medication delivery and real-time tracking are enabled by implanted devices, which are increasingly essential for customized treatment. Pharmacokinetics can be precisely managed through these systems' ability to dynamically and continuously control treatment administration and monitor drug concentrations in the blood (244). In a family Alzheimer's disease model, a sophisticated wearable system has shown the capacity to reduce brain amyloid deposits and improve cognitive function, indicating that wearable ultrasonic devices may provide both therapeutic and diagnostic advantages for neurodegenerative diseases (245).

Ultrasound-triggered immunotherapy and precision medicine

In precision medicine, theranostic platforms that combine

therapeutic and diagnostic capabilities are gaining popularity, particularly for immunotherapy. These technologies allow for adaptive therapy modification based on imaging input and real-time monitoring of treatment response (246). In particular, precise spatial and temporal control over the release of medication or genes has been achieved using ultrasound-responsive hydrogels. These hydrogels enable targeted, on-demand administration of therapeutic drugs, such as chemotherapeutics like doxorubicin, siRNA, or CRISPR/Cas9 complexes, in response to acoustic cues (247). Early theranostic techniques based on ultrasound used targeted microbubbles that carried payloads of miRNA or DNA. These microbubbles rupture in response to ultrasonic stimulation, enhancing tissue permeability and encouraging the absorption of their contents (248, 249). Such treatments, such as microbubbles that target VCAM-1 to release miR-126, have been used in preclinical research to halt the growth of abdominal aortic aneurysms (250, 251).

Multi-modal theranostic systems

In nuclear medicine, theranostics, the combination of targeted treatment with diagnostic imaging has been extensively explored. Examples include paired radiotracer imaging and applications of radionuclide therapy (e.g., thyroid cancer, neuroblastoma)(252-254). Ultrasound-activated contrast compounds are becoming part of emerging multimodal theranostic platforms that go beyond nuclear medicine. Microbubble contrast media, for instance, may release therapeutic chemicals when stimulated by ultrasound and preferentially accumulate in hyper vascular tissues, providing both targeted treatment and diagnostic imaging (255, 256). Additionally, combinations of molecular targeting (e.g., monoclonal antibodies attached to iron oxide nanoparticles) enable site-specific drug release and imaging (via MRI), thereby improving treatment monitoring and specificity, particularly in cancer (257-259).

Future perspective

Future perspectives of ultrasound enhanced by AI

Ultrasound, a historically operator-dependent real-time imaging technique, is being transformed by AI into a more intelligent, independent, and generally accessible diagnostic tool. AI systems may help with activities such as directing picture capture, automating diagnosis, and producing clinical reports thanks to advances in deep learning, computer vision, and natural language processing (260).

Enhanced diagnostic accuracy and consistency

The decrease in operator-dependent variability is one of the main advantages AI provides for ultrasound. Depending on the sonographer's level of experience, conventional ultrasound results might vary considerably (261). To improve consistency and picture quality, AI-driven tools may now automatically deploy probes, adjust imaging parameters, and instantly detect bad scan planes (262). This guarantees more consistent, repeatable imaging, which is particularly important in extensive screening programs such as echocardiography or prenatal abnormality identification (263).

Democratization of ultrasound in low-resource settings

Ultrasound technology is becoming more accessible and smaller thanks to AI. High-quality diagnostic pictures may be obtained and interpreted by non-specialists, such as nurses, midwives, and field health workers, thanks to portable ultrasound probes, cellphones, and integrated AI algorithms (264). In areas with limited resources and a shortage of skilled sonographers, this concept is revolutionizing maternal healthcare. Google's AI ultrasound model, for example, showed that even inexperienced users can reliably take pictures to determine the baby's position and gestational age (265, 266).

Integration with telemedicine and remote care

The integration of portable ultrasound equipment into telemedicine systems has been enabled by AI-guided image capture and analysis. This connection helps reduce healthcare inequities between urban and rural areas by allowing distant experts to analyze AI-assisted scans almost instantly (267, 268). These systems are beneficial for disaster relief, emergency treatment, and home monitoring of long-term conditions like heart failure (269).

AI-driven robotic ultrasound systems

More and more robotic arms with AI capabilities are being developed to perform fully automated ultrasound exams (270). These devices are perfect for repeated monitoring jobs like tracking tumor development or prenatal growth because they provide constant scanning without tiring. They also lessen the exposure of medical personnel to contagious patients, which was a crucial benefit during the COVID-19 epidemic (271).

Automated reporting and clinical workflow optimization

AI is making ultrasound reporting easier by automatically generating standardized, organized reports from collected images. To translate measurements into thorough preliminary reports for physician approval, several systems use natural language generation (260). This decreases transcribing mistakes, cuts down on reporting time, and enhances documentation quality (272, 273).

Medical internet of things (MIoT) and real-time analytics

Continuous data collection, cloud storage, and comprehensive analytics are made possible by the growing integration of AI-powered ultrasound equipment into the Medical Internet of Things (MIoT)(274). Machine learning algorithms may analyze this data to track trends in population health, predict patient decline, and identify early indicators of illness in local areas (275). But these capabilities also present cybersecurity issues that call for strict regulation and strong encryption (273).

New lipid-based microbubbles and ultrasound

Lipid-based microbubbles, combined with ultrasound, offer a versatile platform for targeted tumor therapy, enabling precise drug and gene delivery with minimal systemic toxicity (276, 277). Future research should focus on engineering microbubbles with multifunctional lipid shells capable of carrying therapeutic gases, chemotherapeutics, or nucleic acids, while integrating imaging agents for theranostic applications (278). Advances in ultrasound technology, such as real-time monitoring and adjustable acoustic parameters, will further enhance treatment precision. Moreover, optimizing microbubble stability,

circulation time, and tumor-specific targeting ligands could improve efficacy (279). Translating these innovations into clinical settings will require robust safety profiles, scalable production, and integration with multimodal cancer therapies. The mechanism of Lipid-based microbubbles and ultrasound is shown in Figure 4.

Future challenges and research directions

The integration of AI with ultrasonography presents many challenges that must be addressed.

- Data diversity: Models should be trained on datasets that include a range of demographics, equipment kinds, and clinical settings to guarantee generalizability (265).
- Regulatory approvals: AI systems need stringent validation to comply with FDA, CE, and other regulatory standards (260, 280, 281).
- Clinical acceptance: Physicians must have confidence in AI outputs, necessitating the use of explainable AI (XAI) methodologies to ensure decision transparency (271).
- Integration with current workflows: Systems must be easily incorporated into electronic medical records and PACS without introducing complexity (262).

In the next decade, ultrasound is poised to become an intelligent, multimodal platform that integrates accurate diagnosis, targeted treatment, and immune regulation. Progress in AI will facilitate automated picture acquisition, instantaneous anatomical recognition, and quantitative assessment, diminishing reliance on operators and enhancing accessibility for non-experts. Integrating ultrasound with molecular imaging agents, such as targeted microbubbles or nanobubbles, would provide real-time viewing of essential biomarkers, namely Granzyme B, CD3, and CD4, thereby enhancing early illness identification and continuous therapy assessment.

Ultrasound's mechanical, thermal, and sonochemical properties will be increasingly used for targeted, site-specific administration of pharmaceuticals, genetic material, and immunotherapies. Sonoporation using microbubbles or nanocarriers will enhance intracellular delivery with spatial and temporal precision, while concentrated ultrasound will synergistically augment immune checkpoint inhibitors and cancer vaccines to mitigate immune resistance (214, 217).

The potential of LIPUS in bone regeneration will continue to be demonstrated (187), as will mechanotransduction processes, including integrins, FAK, and Piezo1-mediated Ca^{2+} influx, to heal cartilage and soft tissues (220). Although robust cybersecurity protections will be essential, integration with the Medical Internet of Things (MIoT) will enable remote monitoring, large-scale data analytics, and adaptive therapy optimization. There are still issues, such as standardizing acoustic settings to ensure consistency across devices, overcoming regulatory obstacles, and using clinical validation to verify long-term safety. Despite these challenges, continuous developments at the intersection of biology, engineering, and physics put ultrasonography in a position to evolve from a supplementary imaging modality into a central, intelligent platform for precise, image-guided treatments.

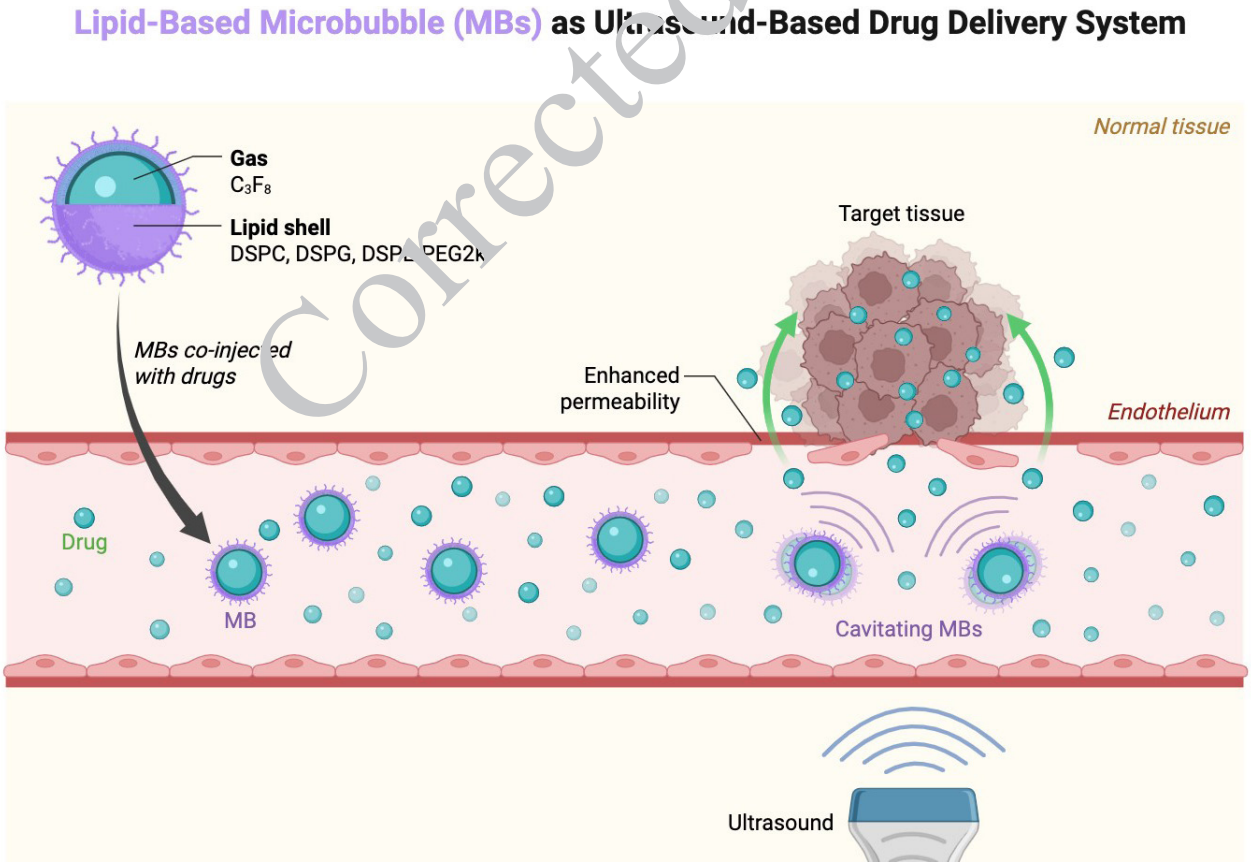

Figure 4. Lipid-based microbubbles as an ultrasound-mediated drug delivery system
Upon ultrasound exposure, lipid-shelled microbubbles can enhance vascular permeability, promote targeted drug release, and facilitate localized delivery of therapeutic agents to tumor sites, minimizing systemic side effects

Long-term toxicity and clearance of nanoparticle radiosensitizers

An essential consideration in the clinical translation of nanoparticle- based radiosensitizers is their long-term fate in the body. Key parameters include biodistribution, retention in non-target organs, degradation or transformation, routes of excretion, and any chronic toxicity or immunological reactions (276, 282-284).

Nanoparticles typically accumulate in reticuloendothelial organs such as the liver, spleen, and kidneys, particularly when their size exceeds ~20-30 nm or when surface coatings enhance opsonization (276). For instance, gold nanoparticles (~20 nm, citrate- or peptide-coated) show rapid redistribution to the liver after intravenous administration, with notable retention even after 28 days, and may occasionally cause mild anemia or splenic atrophy, depending on the coating. In contrast, ultrasmall nanoparticles (<5-6 nm) or metabolizable designs using biodegradable or iron-oxide coatings can undergo renal or metabolic clearance, reducing non-target accumulation and long-term toxicity (283). While some long-term studies, such as 15-month investigations of gold nanorods for photothermal therapy, demonstrate minimal toxicity when particles are well-purified and surface-modified, other reports indicate subtle hematologic or inflammatory effects due to persistent organ accumulation, especially after repeated dosing. Therefore, optimizing nanoparticle size and surface chemistry is essential to enhance clearance and biocompatibility (284). However, most data remain limited to single-dose experiments, with few long-term or large-animal studies assessing chronic exposure, immunogenicity (e.g., anti-coating antibody formation, complement activation), or cumulative toxicity, leaving significant gaps in understanding long-term safety and design strategies (283).

Gaps and key challenges in application areas

In reviewing the literature in ultrasound theranostics, several application areas stand out: cancer therapy (therapy & imaging), blood-brain barrier (BBB) modulation, immunomodulation, and wearable / point-of-care devices. Below, we detail (1) contradictory findings, (2) identified gaps, and (3) pressing translational challenges in each.

Cancer therapy & imaging

Studies on nanoparticle-based radiosensitizers, such as gold nanoparticles, report conflicting outcomes; some demonstrate substantial enhancement of radiotherapy efficacy in tumor models. In contrast, others observe little or no improvement under comparable dose and timing conditions. These inconsistencies often arise from variations in nanoparticle size, surface coating, biodistribution, and tumor vascularization (10, 285). Similarly, HIFU for breast tumor ablation shows initial success in achieving tumor shrinkage, yet follow-up studies reveal variable recurrence rates, likely due to incomplete margin ablation or tissue heterogeneity. Long-term investigations in large animal models or humans remain scarce, and few studies systematically compare nanoparticle formulations or assess off-target tissue effects under standardized ultrasound parameters. Translational challenges persist in ensuring adequate tumor penetration and retention of nanoparticles, overcoming regulatory barriers related to safety and clearance, and improving reproducibility across institutions with differing ultrasound systems and operator expertise. Moreover, integrating reliable imaging guidance and real-time feedback mechanisms is crucial to verify complete tumor ablation during therapy.

Blood-brain barrier (BBB) opening & neurological applications

Contradictory findings

In Alzheimer's models, some studies show that low-intensity ultrasound+microbubbles reduces amyloid burden, improves cognition, or enhances delivery of antibodies; other studies report negligible or even adverse effects depending on microbubble dosage and ultrasound parameters (286). Variability in reported safety: while many animal studies show transient BBB opening without neuronal damage, others report microhemorrhages or edema under certain ultrasound pressures or bubble formulations.

Immunomodulation

Ultrasound (especially with microbubbles or nanoparticles) shows inconsistent immune effects ranging from strong activation of innate and adaptive immunity, enhanced dendritic cell maturation, and improved checkpoint inhibitor efficacy to minimal or variable responses depending on tumor type, dose, and timing. The balance between immune stimulation and suppression remains unclear, as some studies report immunosuppressive tumor microenvironment changes. Mechanistic understanding, including specific immune cell roles, molecular pathways, and optimal sequencing with immunotherapies, is limited. Translational challenges include bridging preclinical models to humans with diverse immune profiles, ensuring safety against excessive inflammation or autoimmunity, and standardizing ultrasound–immunotherapy protocols regarding dose, particle type, and timing.

Wearable/point-of-care & AI-guided systems

AI/ML-based ultrasound radiomics perform well in single-center studies but often lose accuracy in multicenter validation due to variations in devices, operators, and patient populations. Similarly, wearable ultrasound devices show inconsistent performance; some maintain stable signals in motion, while others suffer from artifacts or fidelity loss. Despite the promise, few longitudinal studies have assessed wearable ultrasound for therapeutic monitoring, and robustness under motion, environmental noise, and user variability remains underexplored. Open datasets for AI training, particularly in rare or resource-limited contexts, are scarce. Key translational challenges include ensuring hardware safety and biocompatibility over time, achieving regulatory approval, maintaining data privacy and standardization across platforms, and integrating adaptive feedback loops for real-time monitoring and AI-guided imaging or therapy (287).

Conclusion

Ultrasound medicine has evolved into a flexible theranostic platform that integrates imaging, targeted delivery, and therapeutic modulation. This study has emphasized ultrasound's therapeutic promise, molecular probe synergy, immunological modulation, and regenerative

uses, as well as its mechanical, thermal, and sonochemical processes. Ultrasound improves sensitivity, specificity, and translational effect when paired with MRI, PET/SPECT, and photoacoustic imaging. Despite this development, major issues persist. Reliable clinical application requires standardization of acoustic parameters, improvements in safety thresholds, and repeatable dosimetry. Molecular targeting techniques still have ligand specificity, off-target effects, and immune activation consistency issues. While ultrasonic theranostics has promise in cancer, cardiovascular medicine, and regenerative therapies, large-scale clinical validation is missing. Smart, multifunctional nanocarriers and acoustically responsive biomaterials for precise drug, gene, and immunotherapy delivery, artificial intelligence and real-time monitoring for adaptive, personalized treatment guidance, and standardized protocols and multicenter trials to accelerate regulatory approval and clinical adoption should be the focus of future research. Finally, ultrasound's capacity to combine diagnosis, treatment, and monitoring makes it essential for precision theranostics. Ultrasound might become a cornerstone of image-guided, customized medicine in the future decade by resolving technical and translational constraints.

Acknowledgment

Jiangxi Provincial Health Commission: Study on the predictive value of malignant risk model combined with vaginal endoscopy for endometrial cancer (NO: 202410378).

Funding

No specific funding was received for this work.

Ethical Approval

Not applicable for a review article.

Consent to participate

Not applicable.

Consent to Publish

All authors have agreed to publish in this journal.

Authors' Contributions

L W and Z L conceived and designed the review. L W conducted the literature search and drafted the manuscript. D L contributed to data collection, interpretation, and critical revision of the text. Z L supervised the work and provided final approval of the version to be published. All authors read and approved the final manuscript.

Conflicts of Interest

The authors declare no conflicts of interest related to this article.

Declaration

We acknowledge the use of ChatGPT to improve the main text of the manuscript.

References

1. Bader KB, Padilla F, Haworth KJ, Ellens N, Dalecki D, Miller DL, *et al.* Overview of therapeutic ultrasound applications and safety considerations: 2024 update. J Ultrasound Med 2025; 44: 381-433.
2. Ren J, Li J, Chen S, Liu Y, Ta D. Unveiling the potential of ultrasound in brain imaging: Innovations, challenges, and prospects. Ultrasonics 2025; 145: 107465.
3. Uddin SMZ, Komatsu DE, Motyka T, Petterson S. Low-intensity continuous ultrasound therapies—a systematic review of current state-of-the-art and future perspectives. J Clin Med 2021; 10: 2698.
4. Zhang C, Zhang Q, Xu Q, Jiang X, Ma Y, Liu C, *et al.* Ultrasound targeted microbubbles for theranostic applications in liver diseases: From molecular imaging to targeted therapy. Drug Deliv 2025; 32: 2541656.
5. Jackson SS, Le HM, Kerkhof DL, Corrado GD. Point-of-care ultrasound, the new musculoskeletal physical examination. Curr Sports Med Rep 2021; 20: 109-112.
6. Glass C, Sarwal A, Zavitz J, Nitsche J, Joyner J, Johnson LL, *et al.* Scoping review of implementing a longitudinal curriculum in undergraduate medical education: The wake forest experience. Ultrasound J 2021; 13: 23.
7. Haskins SC, Bronshteyn Y, Perlas A, El-Boghdadly K, Zimmerman J, Silva M, *et al.* American society of regional anesthesia and pain medicine expert panel recommendations on point-of-care ultrasound education and training for regional anesthesiologists and pain physicians-part I: Clinical indications. Reg Anesth Pain Med 2021; 46: 1031-1047.
8. Cid-Serra X, Hoang W, El-Ansary D, Canty D, Royse A, Royse C. Clinical impact of point-of-care ultrasound in internal medicine inpatients: A systematic review. Ultrasound Med Biol 2022; 48: 170-179.
9. Dudek M, Szarpak L, Pecoraro FW, Gasecka A, Michalski T, Wroblewski P, *et al.* Diagnostic performance of point-of-use ultrasound of resuscitation outcomes: A systematic review and meta-analysis of 3,765 patients. Cardiol J 2023; 30: 237-246.
10. Demir ZEF, Sheybani ND. Therapeutic ultrasound for multimodal cancer treatment: A spotlight on breast cancer. Annu Rev Biomed Eng 2025; 27: 371-402.
11. Ding K, Lei J, Zhao Y, Feng Y, Huang H, Hou C. Progress and application of multifunctional ultrasound theranostic agents. Curr Pharm Biotechnol 2025.
12. Zhu K, Wang J, Wang Z, Chen Q, Song J, Chen X. Ultrasound-activated theranostic materials and their bioapplications. Angew Chemie Int Ed 2025; 64: e202422278.
13. Du J, Liao M, Zhang D, Li X. Advanced strategies for ultrasound control and applications in sonogenetics and gas vesicle-based technologies: A review. Int J Nanomedicine 2025; 20: 6533-6549.
14. Xu X, Cao J, Mu Y, Zhang H, Wang YL, Chen M, *et al.* Ultrasound-induced nitric oxide-propelled nanomotor for multimodal theranostics of cancer with deep penetration and extended lifetime. Adv Sci 2025; 12: e16709.
15. Zheng Q, Xia B, Huang X, Luo J, Zhong S, Li X. Nanomedicines for high-intensity focused ultrasound cancer treatment and theranostics (Review). Exp Ther Med 2023; 25: 170.
16. Zhang B, Mo L, Huang R, Chen G, Yang S, Zhang X, *et al.* Ultrasound-enabled sonogenetics: Pioneering advances in cancer theranostics. Adv Funct Mater 2025; 35: 2418748.
17. Martínez-Fernández R, Paschen S, del Álamo M, Rodríguez-Rojas R, Pineda-Pardo JA, Blesa J, *et al.* Focused ultrasound therapy for movement disorders. Lancet Neurol 2025; 24: 698-712.
18. Zhu Z, Zhang Z, Qi G, Li Y, Li Y, Mu L. A dual-branch network for ultrasound image segmentation. Biomed Signal Process Control 2025; 103: 107368.
19. Luijten B, Chennakeshava N, Eldar YC, Mischi M, van Sloun RJG. Ultrasound signal processing: from models to deep learning. Ultrasound Med Biol 2023; 49: 677-698.
20. Yang T, Karakus O, Anantrasirichai N, Achim A. Current advances in computational lung ultrasound imaging: A review. IEEE Trans Ultrason Ferroelectr Freq Control 2023; 70: 2-15.
21. Izadifar Z, Babyn P, Chapman D. Mechanical and biological effects of ultrasound: A review of present knowledge. Ultrasound Med Biol 2017; 43: 1085-1104.
22. Dalecki D. Mechanical bioeffects of ultrasound. Annu Rev Biomed Eng 2004; 6: 229-248.
23. Nightingale K. Acoustic radiation force impulse (ARFI) imaging: A review. Curr Med Imaging Rev 2011; 7: 328-339.

24. Doherty JR, Trahey GE, Nightingale KR, Palmeri ML. Acoustic radiation force elasticity imaging in diagnostic ultrasound. IEEE Trans Ultrason Ferroelectr Freq Control 2013; 60: 685-701.
25. Mohammadjavadi M, Ash RT, Glover GH, Pauly KB. Optimization of MR acoustic radiation force imaging (MR-ARFI) for human transcranial focused ultrasound. Magn Reson Med 2025; 94: 1060-1071.
26. Odéen H, Payne AH, Parker DL. Magnetic resonance acoustic radiation force imaging (MR-ARFI). J Magn Reson Imaging 2025; 62: 20-39.
27. Church CC, Labuda C, Nightingale K. A theoretical study of inertial cavitation from acoustic radiation force impulse imaging and implications for the mechanical index. Ultrasound Med Biol 2015; 41: 472-485.
28. Fowlkes JB, Holland CK. Mechanical bioeffects from diagnostic ultrasound: AIUM consensus statements. American institute of ultrasound in medicine. J ultrasound Med Off J Am Inst Ultrasound Med 2000; 19: 69-72.
29. Quarato CMI, Lacedonia D, Salvemini M, Tuccari G, Mastrodonato G, Villani R, *et al.* A review on biological effects of ultrasounds: Key messages for clinicians. Diagnostics (Basel, Switzerland) 2023; 13: 855.
30. Delalande A, Kotopoulis S, Postema M, Midoux P, Pichon C. Sonoporation: Mechanistic insights and ongoing challenges for gene transfer. Gene 2013; 525: 191-199.
31. Helfield BL, Chen X, Qin B, Watkins SC, Villanueva FS. Mechanistic insight into sonoporation with ultrasound-stimulated polymer microbubbles. Ultrasound Med Biol 2017; 43: 2678-2689.
32. Jiang A, Wang Z, Song D, Zhang X, Guan M, Li X, *et al.* The application of ultrasound-induced blood–brain barrier opening in neurology and immunology. Small 2025; 21: 2502699.
33. Gionso M, Herlin E, Uva L, Guidi F, Tortoli P, Durando G, *et al.* Ultrasound guided blood brain barrier opening using a diagnostic probe in a whole brain model. Sci Rep 2025; 15: 10674.
34. Sun T, Samiotaki G, Wang S, Acosta C, Chen CC, Konofagou EE. Acoustic cavitation-based monitoring of the reversibility and permeability of ultrasound-induced blood-brain barrier opening. Phys Med Biol 2015; 60: 9079-9094.
35. Şen T, Tüfekçioğlu O, Koza Y. Mechanical index. Anatol J Cardiol 2015; 15: 334-336.
36. Bachu VS, Kedda J, Suk I, Green JJ, Tyler B. High-intensity focused ultrasound: A review of mechanisms and clinical applications. Ann Biomed Eng 2021; 49: 1975-1991.
37. Shrivastava D, Vaughan JT. A generic bioheat transfer thermal model for a perfused tissue. J Biomech Eng 2009; 131: 74506.
38. van Rhoon GC, Samaras T, Yarmolenko PS, Dewhirst MW, Neufeld E, Kuster N. CEM43°C thermal dose thresholds: A potential guide for magnetic resonance radiofrequency exposure levels? Eur Radiol 2013; 23: 2215-2227.
39. Santos MA, Goertz DE, Hynynen K. Focused ultrasound hyperthermia mediated drug delivery using thermosensitive liposomes and visualized with *in vivo* two-photon microscopy. Theranostics 2017; 7: 2718-2731.
40. Hijnen N, Kneepkens E, de Smet M, Langereis S, Heijman E, Grüll H. Thermal combination therapies for local drug delivery by magnetic resonance-guided high-intensity focused ultrasound. Proc Natl Acad Sci 2017; 114: E4802-4811.
41. Zhong C, Bai J, Yang X, Ji Y, Huang J, Tan X, *et al.* A study of saponin-encapsulated ultrasound microbubbles Rb 3 NPs@ MBs for atherosclerosis targeted treatment. Biomater Sci 2025; 13: 4984-5000.
42. Tian S, Jiang T, Su M, Su P, Jia Z, Ke L, *et al.* Novel supramolecular self-assembled nanomedicines for ultrasound-triggered tumor programmed therapy. Chem Eng J 2025; 520: 166106.
43. Cai L, Du J, Han F, Shi T, Zhang H, Lu Y, *et al.* Piezoelectric metal-organic frameworks based sonosensitizer for enhanced nanozyme catalytic and sonodynamic therapies. ACS Nano 2023; 17: 7901-7910.
44. Karthika V, Badrinathan Sridharan, Nam JW, Kim D, Gyun Lim H. Neuromodulation by nanozymes and ultrasound during Alzheimer's disease management. J Nanobiotechnology 2024; 22: 139.
45. Cağlı M, Duyur Çakıt B, Pervane S. Efficacy of therapeutic ultrasound added to complex decongestive therapy in breast cancer-related lymphedema. Lymphat Res Biol 2025; 23: 272-280.
46. Yang Y, Sun Y, Mao W wei, Zhang H, Ni B, Jiang L. Oxidative stress induces downregulation of TP53INP2 and suppresses osteogenic differentiation of BMSCs during osteoporosis through the autophagy degradation pathway. Free Radic Biol Med 2021; 166: 226-237.
47. Hu Y, Zhao G, Qin L, Yu Z, Zhang M, Ma X, *et al.* Trans, trans-2, 4-Decadienal induces endothelial cell injury by impairing mitochondrial function and autophagic flux. Food Funct 2021; 12: 5488-5500.
48. Al Refaai KA, AlSawaftah NA, Abuwatfa W, Husseini GA. Drug release via ultrasound-activated nanocarriers for cancer treatment: A review. Pharmaceutics 2024; 16: 1383.
49. Fokong S, Theek B, Wu Z, Koczera P, Appold L, Jorge S, *et al.* Image-guided, targeted and triggered drug delivery to tumors using polymer-based microbubbles. J Control release Off J Control Release Soc 2012; 163: 75-81.
50. Mørch Ý, Hansen R, Berg S, Åslund AKO, Glomm WR, Eggen S, *et al.* Nanoparticle-stabilized microbubbles for multimodal imaging and drug delivery. Contrast Media Mol Imaging 2015; 10: 356-366.
51. Lv Y, Hao L, Hu W, Ran H, Bai Y, Zhang L. Novel multifunctional pH-sensitive nanoparticles loaded into microbubbles as drug delivery vehicles for enhanced tumor targeting. Sci Rep 2016; 6: 29321.
52. Chang CF, Lin CW, Yeh CK. Ultrasound-triggered drug release and cytotoxicity of microbubbles with diverse drug attributes. Ultrason Sonochem 2025; 112: 107182.
53. Han Y, Wang F, Shen J, Chen S, Xiao P, Zhu Y, *et al.* Ultrasound nanobubble coupling agent for effective noninvasive deep-layer drug delivery. Adv Mater 2024; 36: 2306993.
54. Cui R, Zhou J, Yang W, Chen Y, Chen L, Tan L, *et al.* Ultrasound-triggered nanogel boosts chemotherapy and immunomodulation in colorectal cancer. ACS Appl Mater Interfaces 2025; 17: 211-221.
55. Nittayacharn P, Abenojar E, Cooley MB, Berg FM, Counil C, Sojahrood AJ, *et al.* Efficient ultrasound-mediated drug delivery to orthotopic liver tumors–Direct comparison of doxorubicin-loaded nanobubbles and microbubbles. J Control Release 2024; 367: 135-147.
56. Furusawa Y, Hassan MA, Zhao QL, Ogawa R, Tabuchi Y, Kondo T. Effects of therapeutic ultrasound on the nucleus and genomic DNA. Ultrason Sonochem 2014; 21: 2061-2068.
57. Przystupski D, Ussowicz M. Landscape of cellular bioeffects triggered by ultrasound-induced sonoporation. Int J Mol Sci 2022; 23: 11222.
58. Elsner HI, Lindblad EB. Ultrasonic degradation of DNA. DNA 1989; 8: 697-701.
59. Costello M, Pugh TJ, Fennell TJ, Stewart C, Lichtenstein L, Meldrim JC, *et al.* Discovery and characterization of artifactual mutations in deep coverage targeted capture sequencing data due to oxidative DNA damage during sample preparation. Nucleic Acids Res 2013; 41: e67.
60. Harle J, Mayia F, Olsen I, Salih V. Effects of ultrasound on transforming growth factor-beta genes in bone cells. Eur Cell Mater 2005; 10: 70-76.
61. Hasanova GI, Noriega SE, Mamedov TG, Thakurta SG, Turner JA, Subramanian A. The effect of ultrasound stimulation on the gene and protein expression of chondrocytes seeded in chitosan scaffolds. J Tissue Eng Regen Med 2011; 5: 815-822.
62. Filieri S, Miciaccia M, Armenise D, Baldelli OM, Liturri A, Ferorelli S, *et al.* Can focused ultrasound overcome the failure of chemotherapy in treating pediatric diffuse intrinsic pontine glioma due to a blood-brain barrier obstacle? Pharmaceuticals (Basel) 2025; 18: 525.
63. McKee JR, Christman CL, O'Brien Jr WD, Wang SY. Effects of ultrasound on nucleic acid bases. Biochemistry 1977; 16: 4651-

4654.
64. Pinamonti S, Caruso A, Mazzeo V, Zebini E, Rossi A. DNA damage from pulsed sonication of human leukocytes *in vitro*. IEEE Trans Ultrason Ferroelectr Freq Control 1986; 33 :179-185.
65. Miller DL, Reese JA, Frazier ME. Single strand DNA breaks in human leukocytes induced by ultrasound *in vitro*. Ultrasound Med Biol 1989; 15: 765-771.
66. Miller DL, Thomas RM, Frazier ME. Ultrasonic cavitation indirectly induces single strand breaks in DNA of viable cells *in vitro* by the action of residual hydrogen peroxide. Ultrasound Med Biol 1991; 17: 729-735.
67. Miller DL, Thomas RM, Frazier ME. Single strand breaks in CHO cell DNA induced by ultrasonic cavitation *in vitro*. Ultrasound Med Biol 1991;17: 401–406.
68. Kondo T, Arai S, Kuwabara M, Yoshii G, Kano E. Damage in DNA irradiated with 1.2 MHz ultrasound and its effect on template activity of DNA for RNA synthesis. Radiat Res 1985; 104: 284-292.
69. Bonner WM, Redon CE, Dickey JS, Nakamura AJ, Sedelnikova OA, Solier S, *et al.* GammaH2AX and cancer. Nat Rev Cancer 2008; 8: 957-967.
70. Ward IM, Chen J. Histone H2AX is phosphorylated in an ATR-dependent manner in response to replicational stress. J Biol Chem 2001; 276: 47759-47762.
71. Stiff T, O'Driscoll M, Rief N, Iwabuchi K, Löbrich M, Jeggo PA. ATM and DNA-PK function redundantly to phosphorylate H2AX after exposure to ionizing radiation. Cancer Res 2004; 64: 2390–2396.
72. Furusawa Y, Fujiwara Y, Campbell P, Zhao QL, Ogawa R, Hassan MA, *et al.* DNA double-strand breaks induced by cavitational mechanical effects of ultrasound in cancer cell lines. PLoS One 2012; 7: e29012.
73. Liu S, Li M, Guo Z, Chen Z. Exploring the molecular mechanism of cancer radiosensitization: The impact of physical stimulation therapy. Strahlentherapie und Onkol 2025; 201: 1058-1070.
74. Abdollahi A, Domhan S, Jenne JW, Hallaj M, Dell'Aqua G, Mueckenthaler M, *et al.* Apoptosis signals in lymphoblasts induced by focused ultrasound. FASEB J Off Publ Fed Am Soc Exp B[illegible] 2004; 18: 1413-1414.
75. Furusawa Y, Kondo T. DNA damage induced by ultrasound and cellular responses. Mol Biol 2017; 6: 2.
76. Chen X, Wan JMF, Yu ACH. Sonoporation as a cellular stress: Induction of morphological repression and developmental delays. Ultrasound Med Biol 2013; 39: 1075-1086.
77. Hassan MA, Furusawa Y, Minemura M, Rapoport N, Sugiyama T, Kondo T. Ultrasound-induced new cellular mechanism involved in drug resistance. PLoS One 2012; 7: e41291.
78. Leone P, Malerba E, Susca N, Favoino E, Perosa F, Brunori G, *et al.* Endothelial cells in tumor microenvironment: Insights and perspectives. Front Immunol 2024; 15: 1367875.
79. Li Z, Zhang B, Duan S, Liu R, Wang Y, Wang Y, *et al.* Ultrasound-activated nanovesicles for adenosine exhaustion and immune checkpoint blockade in cancer immunotherapy. J Control Release 2025; 385: 113988.
80. Anderson NM, Simon MC. The tumor microenvironment. Curr Biol 2020; 30: R921-925.
81. Wang MJ, Graf-Alexiou ML, Nguyen DKCT, Hoang MTH, Major PP, Le PLH. A study of accuracy and reliability of intraoral ultrasound using *ex vivo* and *in vivo* data. Oral Surg Oral Med Oral Pathol Oral Radiol. 2025; 139: e96.
82. Park K, Veena MS, Shin DS. Key players of the immunosuppressive tumor microenvironment and emerging therapeutic strategies. Front cell Dev Biol 2022; 10: 830208.
83. Zhang J, Luan X, Lv Z, Wang Y, Yu Q, Zhong H, *et al.* Electron transfer driven piezocatalytic degradation of emerging contaminants: Recent advances, modification strategies, and prospects. J Water Process Eng 2025; 75: 108012.
84. Musiu C, Lupo F, Agostini A, Lionetto G, Bevere M, Paiella S, *et al.* Cellular collusion: Cracking the code of immunosuppression and chemo resistance in PDAC. Front Immunol 2024; 15: 1341079.
85. Singh A, Tijore A, Margadant F, Simpson C, Chitkara D, Low BC, *et al.* Enhanced tumor cell killing by ultrasound after microtubule depolymerization. Bioeng Transl Med 2021; 6: e10233.
86. Tijore A, Margadant F, Dwivedi N, Morgan L, Yao M, Hariharan A, *et al.* Ultrasound-mediated mechanical forces activate selective tumor cell apoptosis. Bioeng Transl Med 2025; 10: e10737.
87. Lejbkowicz F, Zwiran M, Salzberg S. The response of normal and malignant cells to ultrasound in vitro. Ultrasound Med Biol 1993; 19: 75–82.
88. Huang S, Cheng C, Wang Z, Li R, Li W, Yu K, *et al.* Low-intensity-pulsed-ultrasound-treated menstrual-blood-derived mesenchymal stem cells repair endometrial injury by PI3K/AKT pathway inhibition. Reprod Biomed Online 2025; 50: 104486.
89. Xie X, Zhang J, Wang Y, Shi W, Tang R, Tang Q, *et al.* Nanomaterials augmented bioeffects of ultrasound in cancer immunotherapy. Mater Today Bio 2024; 24: 100926.
90. Zhang J, Sun L, Jiang L, Xie X, Wang Y, Wu R, *et al.* Regulation of CTLs/Tregs via highly stable and ultrasound-responsive cerasomal nano-modulators for enhanced colorectal cancer immunotherapy. Adv Sci 2024; 11: 2400485.
91. Baez A, Singh D, He S, Hajiaghayi M, Gholizadeh F, Darlington PJ, *et al.* Immunomodulation of human T cells by microbubble-mediated focused ultrasound. Front Immunol 2024; 15: 1486744.
92. Campanelli R, Carolei A, Catarsi P, Abbà C, Boveri E, Paulli M, *et al.* Circulating polymorphonuclear myeloid-derived suppressor cells (PMN-MDSCs) have a biological role in patients with primary myelofibrosis. Cancers 2024; 16: 2556.
93. Zhou LX, Jiang YZ, Li XQ, Zhang JM, Li SP, Wei L, *et al.* Myeloid-derived suppressor cells-induced exhaustion of CD^{8+} T-cell participates in rejection after liver transplantation. Cell Death Dis 2024; 15: 307.
94. Pellegatta S, Corradino N, Zingarelli M, Porto E, Gionso M, Poliani PL, *et al.* The immunomodulatory effects of fluorescein-mediated sonodynamic treatment lead to systemic and intratumoral depletion of myeloid-derived suppressor cells in a preclinical malignant glioma model. Cancers 2024; 16: 792.
95. Huang D, Xu M, Wang H, Zhao Y, Zhang Z, Yu M, *et al.* SIRPα blockade therapy potentiates immunotherapy by inhibiting PD-L1+ myeloid cells in hepatocellular carcinoma. Cell Death Dis 2025; 16: 451.
96. Huang Z, Yue JQ, Zhu RH, Xin JY, Luo HC, Li KY. Perfluorobutane-enhanced US Targeting M2 Tumor-associated Macrophages for Predicting Programmed Cell Death-1 Response in Hepatocellular Carcinoma. Radiol Imaging Cancer 2025; 7: e240472.
97. Alva A, Kim C, Premdas P, Ferry Y, Lee H, Lal N, *et al.* Imaging of macrophage accumulation in solid tumors with ultrasound. Nat Commun 2025; 16: 6322.
98. Fu Z, Zhang L, Chen R, Zhan J, Zhong J, Zheng W, *et al.* Biphasic co-detection of melanoma aneuploid tumor cells and tumor endothelial cells in guidance of specifying the field cancerized surgical excision margin and administering immunotherapy. Cancer Lett 2024; 598: 217099.
99. Chinigò G, Scarpellino G, Petrillo S, Genova T, Ruffinatti FA, Munaron L. Modulation of purinergic signaling in endothelial cells by tumor microenvironment. Vascul Pharmacol 2024; 155: 107311.
100. Sadeghipour N, Tabesh F, Natarajan A, Lutz A, Paulmurugan R, Kaffas A El. Molecular ultrasound imaging of PD-L1 expression on cancer endothelial cells. Ultrasound Med Biol 2025; 51: 1675-1681.
101. Changizi S, Marquette IG, VanSant J, Alghazwat O, Elgattar A, Liao Y, *et al.* Carbon monoxide release from ultrasound-sensitive microbubbles improves endothelial cell growth. J Biomed Mater Res Part A 2024; 112: 600–612.
102. Mai Z, Lin Y, Lin P, Zhao X, Cui L. Modulating extracellular matrix stiffness: A strategic approach to boost cancer immunotherapy. Cell Death Dis 2024; 15: 307.
103. Lin N, Yang Z, Yi W, Chen Y, Lai F. Delving into immune modulation: Thymectomy in myasthenia gravis. J Cardiothorac Surg 2025; 20: 277.

104. Guipaud O, Lago C, Portier L, Paget V, François A, Supiot S, *et al.* Exploiting the endothelial-immune axis to improve radiotherapy efficacy. Br J Radiol 2025; 98: 1176-1187.
105. He M, Zhu H, Dong J, Lin W, Li B, Li Y, *et al.* Low-intensity pulsed ultrasound improves metabolic dysregulation in obese mice by suppressing inflammation and extracellular matrix remodeling. Ultrasonics 2025; 145: 107488.
106. Huang R, Zhang B, Chen G, Zhao Y, Wang R, Zhu H, *et al.* Ultrasound-mediated FAK-targeted nano-sapper for tumor extracellular matrix remodeling to potentiate cancer immunotherapy. Chem Eng J 2025; 515: 163837.
107. Yilmaz AÇ, Toktas H, Celik S, Sen S. Therapeutic ultrasound modulates cell proliferation and proinflammatory cytokine levels in osteoarthritic chondrocytes. J Cell Mol Med 2025; 29: e70257.
108. de Araújo Alves CC, de Melo PF, Vieira L, Mathur S, Burtin C, Maldaner VZ, *et al.* Early detection of muscle wasting assessed by ultrasound and analysis of growth factor and systemic inflammation mediators in critically ill trauma patients: An observational study. Eur J Trauma Emerg Surg 2025; 51: 93.
109. Zhang C, Chen Y, Han J, Liu R, Liu C, Zhao Y, *et al.* Ultrasound nanobubble-based combinational strategies of loaded miR-107-3p and CD133 Ab for anti-PD-L1 and anti-hepatocellular cancer stem cells. Int J Pharm 2025; 670: 125140.
110. Yamaguchi T, Endo-Takahashi Y, Awaji K, Numazawa S, Onishi Y, Tada R, *et al.* Microfluidic nanobubbles produced using a micromixer for ultrasound imaging and gene delivery. Sci Rep 2025; 15: 14871.
111. Patil C, Priyanka R, Harshitha BM, Oshik S, Yashwanth S, Darshan BR, *et al.* Advanced nanotheranostic approaches for targeted glioblastoma treatment: A synergistic fusion of CRISPR-Cas gene editing, AI-driven tumor profiling, and BBB-modulation. Med Oncol 2025; 42: 413.
112. Hazel K, Singh D, He S, Guertin Z, Husser MC, Helfield B. Focused ultrasound and microbubble-mediated delivery of CRISPR-Cas9 ribonucleoprotein to human induced pluripotent stem cells. Mol Ther 2025; 33: 986-996.
113. Song J, Parakhonskiy B V, Skirtach AG. Energy transfer influence on superfast calcium carbonate synthesis: Using microwave heating, ultrasound cavitation and mechanical stirring. J Mater Res Technol 2025; 35: 5600–5613.
114. Careaga J, Nikolić V, Said-Houari B. Westervelt-based modeling of ultrasound-enhanced drug delivery. J Nonlinear Sci 2025; 35: 61.
115. Sharma D, Czarnota GJ. Using ultrasound and microbubble to enhance the effects of conventional cancer therapies in clinical settings. Cancer Metastasis Rev 2025; 44: 39.
116. Han L, Dai Q, He C, Xu J, Cui L, Xie X, *et al.* A tetrahedral DNA nanoplatform with ultrasound-triggered biomimetic nanocarriers for targeted siMCM2 delivery and reversal of imatinib resistance in gastrointestinal stromal tumors. Chem Eng J 2025; 504: 158843.
117. Kaushik A, Fabiilli ML, Myers DD, Fowlkes JB, Aliabouzar M. Advancing acoustic droplet vaporization for tissue characterization using quantitative ultrasound and transfer learning. IEEE Trans Biomed Eng 2025; 72: 1897-1908.
118. Song Y, Wang Y, Wang W, Xie Y, Zhang J, Liu J, *et al.* Advancements in noninvasive techniques for transplant rejection: From biomarker detection to molecular imaging. J Transl Med 2025; 23: 147.
119. Morawski AM, Lanza GA, Wickline SA. Targeted contrast agents for magnetic resonance imaging and ultrasound. Curr Opin Biotechnol 2005; 16: 89–92.
120. Weller GER, Lu E, Csikari MM, Klibanov AL, Fischer D, Wagner WR, *et al.* Ultrasound imaging of acute cardiac transplant rejection with microbubbles targeted to intercellular adhesion molecule-1. Circulation 2003; 108:2 18–224.
121. Jin Y, Gao P, Liang L, Wang Y, Li J, Wang J, *et al.* Noninvasive quantification of granzyme B in cardiac allograft rejection using targeted ultrasound imaging. Front Immunol 2023; 14: 1164183.
122. Hou L, Guo Z, Liu S, Liang X, Du M, Chen Z. Ultrasound molecular imaging with VEGFR2 Targeted microbubbles to evaluate intrauterine adhesion after endometrial injury and monitor the therapeutic effects. J Ultrasound Med 2025; 44: 1555–1568.
123. Liu J, Chen Y, Wang G, Lv Q, Yang Y, Wang J, *et al.* Ultrasound molecular imaging of acute cardiac transplantation rejection using nanobubbles targeted to T lymphocytes. Biomaterials 2018; 162: 200–207.
124. Liang M, Kang X, Liu H, Zhang L, Wang T, Ye M, *et al.* Ultrasound-energized OX40L-expressing biohybrid for multidimensional mobilization of sustained T cell-mediated antitumor immunity and potent sono-immunotherapy. J Am Chem Soc 2025; 147: 13833–13850.
125. Li J, Wen L, Guo Y, Yao D, Sun B, Mou H, *et al.* Combination of low-intensity pulsed ultrasound irradiating immune organs with immune checkpoint blockade augments systemic anti-tumor immunity on low tumor burden 4T-1 breast cancer. Cancer Immunol Immunother 2025; 74: 281.
126. Liao T, Liu X, Ren J, Zhang H, Zheng H, Li X, *et al.* Noninvasive and quantitative measurement of C4d deposition for the diagnosis of antibody-mediated cardiac allograft rejection. EBioMedicine 2018; 37: 236–245.
127. Kardani H, Vaghani H, Patel P, Kumbhani J. Green synthesis of hydrazone-linked 1,2,3-triazole-coumarin hybrids via ultrasound: *In vitro* and *in silico* DNA gyrase inhibition studies. ChemistrySelect 2025; 10: e029..9.
128. Mahmood U, Josephson L. Molecular MR imaging probes. Proc IEEE 2005; 93: 800–808.
129. Aherne T, Tschakaloff D, Finkbeiner W, Sechtem U, Derugin N, Yee E, *et al.* Magnetic resonance imaging of cardiac transplants: The evaluation of rejection of cardiac allografts with and without immunosuppression. Circulation 1986; 74: 145-156.
130. Maheshwari S, Singh A, Verma A, Shariq M, Akhtar J, Alsaidan OA, *et al.* Superparamagnetic iron oxide nanoparticles (SPIONs) in targeting brain tumors: Advances and challenges. Med Oncol 2025 ; 42: 338.
131. Wu YL, Ye Q, Foley LM, Hitchens TK, Sato K, Williams JB, *et al. In situ* labeling of immune cells with iron oxide particles: An approach to detect organ rejection by cellular MRI. Proc Natl Acad Sci U S A 2006; 103: 1852–1857.
132. Toki D, Zhang W, Hor KLM, Liuwantara D, Alexander SI, Yi Z, *et al.* The role of macrophages in the development of human renal allograft fibrosis in the first year after transplantation. Am J Transplant 2014; 14: 2126-2136.
133. Salehi S, Reed EF. The divergent roles of macrophages in solid organ transplantation. Curr Opin Organ Transplant 2015; 20: 446-453.
134. Ye Q, Wu YL, Foley LM, Hitchens TK, Eytan DF, Shirwan H, *et al.* Longitudinal tracking of recipient macrophages in a rat chronic cardiac allograft rejection model with noninvasive magnetic resonance imaging using micrometer-sized paramagnetic iron oxide particles. Circulation 2008; 118: 149-156.
135. Dolan RS, Rahsepar AA, Blaisdell J, Suwa K, Ghafourian K, Wilcox JE, *et al.* Multiparametric cardiac magnetic resonance imaging can detect acute cardiac allograft rejection after heart transplantation. JACC Cardiovasc Imaging 2019; 12: 1632-1641.
136. Liu L, Ye Q, Wu Y, Hsieh WY, Chen CL, Shen HH, *et al.* Tracking T-cells *in vivo* with a new nano-sized MRI contrast agent. Nanomedicine 2012; 8: 1345–1354.
137. Giannakodimos I, Kaltsas A, Moulavasilis N, Kratiras Z, Mitropoulos D, Chrisofos M, *et al.* Fusion MRI/ultrasound-guided transperineal biopsy: A game changer in prostate cancer diagnosis. J Clin Med 2025; 14: 453.
138. Ge J, Zhang Q, Zeng J, Gu Z, Gao M. Radiolabeling nanomaterials for multimodality imaging: New insights into nuclear medicine and cancer diagnosis. Biomaterials 2020; 228: 119553.
139. Eichendorff S, Svendsen P, Bender D, Keiding S, Christensen EI, Deleuran B, *et al.* Biodistribution and PET imaging of a novel [68Ga]-anti-CD163-antibody conjugate in rats with collagen-induced arthritis and in controls. Mol imaging Biol 2015; 17: 87-

93.
140. Fiordelisi MF, Auletta L, Meomartino L, Basso L, Fatone G, Salvatore M, *et al.* Preclinical molecular imaging for precision medicine in breast cancer mouse models. Contrast Media Mol Imaging 2019; 2019: 8946729.
141. O'Neill ASG, Terry SYA, Brown K, Meader L, Wong AMS, Cooper JD, *et al.* Non-invasive molecular imaging of inflammatory macrophages in allograft rejection. EJNMMI Res 2015; 5: 69.
142. Li H, Chen Y, Jin Q, Wu Y, Deng C, Gai Y, *et al.* Noninvasive radionuclide molecular imaging of the CD4-positive T lymphocytes in acute cardiac rejection. Mol Pharm 2021; 18: 1317–1326.
143. Sharif-Paghaleh E, Yap ML, Meader LL, Chuamsaamarkkee K, Kampmeier F, Badar A, *et al.* Noninvasive imaging of activated complement in ischemia-reperfusion injury post-cardiac transplant. Am J Transplant 2015; 15: 2483–2490.
144. Bhatnagar A, Narula J. Radionuclide imaging of cardiac pathology: A mechanistic perspective. Adv Drug Deliv Rev 1999; 37: 213-223.
145. Grabner A, Kentrup D, Edemir B, Sirin Y, Pavenstädt H, Schlatter E, *et al.* PET with 18F-FDG-labeled T lymphocytes for diagnosis of acute rat renal allograft rejection. J Nucl Med 2013; 54: 1147–1153.
146. Konishi M, Erdem SS, Weissleder R, Lichtman AH, McCarthy JR, Libby P. Imaging granzyme B activity assesses immune-mediated myocarditis. Circ Res 2015; 117: 502–512.
147. Larimer BM, Wehrenberg-Klee E, Dubois F, Mehta A, Kalomeris T, Flaherty K, *et al.* Granzyme B PET imaging as a predictive biomarker of immunotherapy response. Cancer Res 2017; 77: 2318–2327.
148. Schwenck J, Sonanini D, Cotton JM, Rammensee HG, la Fougère C, Zender L, *et al.* Advances in PET imaging of cancer. Nat Rev Cancer 2023; 23: 474–490.
149. Daly KP, Dearling JLJ, Seto T, Dunning P, Fahey F, Packard AB, *et al.* Use of [18F]FDG positron emission tomography to monitor the development of cardiac allograft rejection. Transplantation 2015; 99: e132-139.
150. Ueno T, Dutta P, Keliher E, Leuschner F, Majmudar M, Marinelli B, *et al.* Nanoparticle PET-CT detects rejection and immunomodulation in cardiac allografts. Circ Cardiovasc Imaging 2013; 6: 568–573.
151. Lohmann P, Schäfer L, Krause S, Altunay B, Wilhelmi A, Werner JM, *et al.* Advancements in non-invasive visualization of the immune environment in glioblastoma: A systematic review. Neuro-Oncology Adv 2025; 7: vdaf176.
152. Taşdelen E, Kutlay NY, Kaplan İ, Altıner S, Akay M T. Association between OX40L rs1234314 and rs2146838 polymorphisms and unexplained recurrent pregnancy loss. Mol Biol Rep 2025; 52: 548.
153. Hirai T, Mayer AT, Nobashi TW, Lin FY, Xiao Z, Udagawa T, *et al.* Imaging alloreactive T cells provides early warning of organ transplant rejection. JCI insight 2021; 6: e145360.
154. Dar O, Dulay MS, Riesgo-Gil F, Morley-Smith A, Brookes P, Lyster H, *et al.* Cardiac transplant rejection assessment with 18F-FDG PET-CT: Initial single-centre experience for diagnosis and management. EJNMMI Rep 2024; 8: 9.
155. Li B, Zhao X, Luo S, Zhong Q, Zhao H, Du C, *et al.* Preoperative localization of parathyroid glands in secondary hyperparathyroidism: Correlations between 99mTc-MIBI-SPECT/CT, ultrasound, and pathological characteristics. Clin Kidney J 2025; 18: sfaf040.
156. Liu T, Wang J, Cui T, Yang L, Li Z, Yan F. Targeted biosynthetic nanobubbles for ultrasound molecular imaging of prostate cancer. Ultrasound Med Biol 2025; 51: 1447–1458.
157. Sheth M, Knight C, Wu Q, Vasilyeva A, Upadhyay A, Bau L, *et al.* Size matters: Micro- versus nanobubbles in ultrasound imaging and therapy. Sci Adv 2025; 11: eads2177.
158. Wegierak D, Nittayacharn P, Cooley MB, Berg FM, Kosmides T, Durig D, *et al.* Nanobubble contrast enhanced ultrasound imaging: A review. Wiley Interdiscip Rev Nanomed Nanobiotechnol 2024; 16: e2007.
159. Kulkarni AD, Mukarrama T, Barlow BR, Kim J. Recent advances in non-invasive *in vivo* tracking of cell-based cancer immunotherapies. Biomater Sci 2025; 13: 1939–1959.
160. Cen P, Luo X, Wang J, Chen H, Tian M, Zhang H. Molecular imaging of stem cell therapies in ischemic stroke. Eur J Nucl Med Mol Imaging 2025; 53: 71-92.
161. Leder T, Seifert P, Gühne F, Freesmeyer M. Simultaneous identification of Tc-99m-sestamibi-positive autonomous thyroid adenoma and adjacent F-18-ethylcholine-positive parathyroid adenoma in patient with graves' disease using real-time ultrasound fusion imaging. Diagnostics 2025; 15: 1262.
162. Sriwastwa A, Trout AT, Mahoney BW, Wang LL, Scheler JL. Nuclear medicine imaging in epilepsy. RadioGraphics 2025; 45: e240062.
163. Zamani-Siahkali N, Mirshahvalad SA, Farbod A, Divband G, Pirich C, Veit-Haibach P, *et al.* SPECT/CT, PET/CT, and PET/MRI for response assessment of bone metastases. Semin Nucl Med 2024; 54: 356–3570.
164. Yang L, Gao T, Huang Y, Wang P he, Han X hao, Wu J, *et al.* Ultrasound-targeted β-catenin gene therapy improves the cardiac function in mice after myocardial infarction. Cardiovasc Toxicol 2025; 25: 74–84.
165. Tang S, McGinnis R, Cao Z, Baker JR, Xu Z, Wang S. Ultrasound-guided histotripsy triggers the release of tumor-associated antigens from breast cancer. Cancers 2025; 17: 183.
166. Wang L, Cao L, Shao K, Su J, Li G, Wang C, *et al.* Phytochlorin-based sonosensitizers combined with free-field ultrasound for immune-sonodynamic cancer therapy. Adv Mater 2025; 37: 2410559.
167. Casenghi M, Poletti E, Popolo Rubbio A, Brambilla N, Testa L, Bedogni F, *et al.* [Transcatheter aortic valve implantation for pure aortic regurgitation]. G Ital Cardiol (Rome) 2021; 22: 21S-28S.
168. Wu Q, Xia J, Xiong X, Duan X, Pang X, Zhang F, *et al.* Focused ultrasound-mediated small-molecule delivery to potentiate immune checkpoint blockade in solid tumors. Front Pharmacol 2023; 14: 1169608.
169. Liu S, Zhang Y, Liu Y, Wang W, Gao S, Yuan W, *et al.* Ultrasound-targeted microbubble destruction remodels tumour microenvironment to improve immunotherapeutic effect. Br J Cancer 2023; 128: 715-725.
170. Liu D, Ling Y, Dong L, Zhang J, Li X, Chen X, *et al.* Ultrasound-triggered drug-loaded nanobubbles for enhanced T cell recruitment in cancer chemoimmunotherapy. Biomaterials 2025; 317: 123086.
171. Deng J, Zhang Y, Feng J, Wu F. Dendritic cells loaded with ultrasound-ablated tumour induce *in vivo* specific antitumour immune responses. Ultrasound Med Biol 2010; 36: 441–448.
172. Liao Y, Wang D, Yang X, Ni L, Lin B, Zhang Y, *et al.* High-intensity focused ultrasound thermal ablation boosts the efficacy of immune checkpoint inhibitors in advanced cancers with liver metastases: A single-center retrospective cohort study. Oncol Lett 2025; 29: 124.
173. Hawley JJ, Allen SL, Thompson DM, Schwarz AJ, Tranquart FJM. Commercially available ultrasound contrast agents: Factors contributing to favorable outcomes with ultrasound-mediated drug delivery and ultrasound localization microscopy imaging. Invest Radiol 2025; 60: 813-822.
174. Exner AA, Escoffre JM. Editorial: Biomedical advances in ultrasound-mediated drug/molecule delivery. Front Pharmacol 2022; 13: 974921.
175. Cai X, Liu Y, Luo G, Yu Z, Jiang C, Xu C. Ultrasound-assisted immunotherapy for malignant tumour. Front Immunol 2025; 16: 1547594.
176. Unga J, Hashida M. Ultrasound induced cancer immunotherapy. Adv Drug Deliv Rev 2014; 72: 144–153.
177. Yan Ruiqian, Li Haixia, Gao Junxi. Relationship between the ultrasound features of different molecular subtypes of breast cancer and positive PD-1/PD-L1 expression. J Int Med Res 2025; 53: 03000605251314812.
178. Dahan M, Cortet M, Lafon C, Padilla F. Combination of focused ultrasound, immunotherapy, and chemotherapy. J

Ultrasound Med 2022; 42: 559-573.
179. Hu C, Li H, Deng T, Liu Z, Yang L, Peng L, *et al.* Abscopal effect of focused ultrasound combined immunotherapy in animal solid tumor model: A systematic reviews and meta-analysis. Front Immunol 2024; 15: 1474343.
180. Joiner JB, Pylayeva-Gupta Y, Dayton PA. Focused ultrasound for immunomodulation of the tumor microenvironment. J Immunol 2020; 205: 2327-2341.
181. Zhou Y, Pang L, Ding T, Chen K, Liu J, Wu M, *et al.* Precise *in situ* delivery of a photo-enhanceable inflammasome-activating nanovaccine activates anticancer immunity. Cancer Res 2024; 84: 3834–3847.
182. Zhang Y, Deng J, Feng J, Wu F. Enhancement of antitumor vaccine in ablated hepatocellular carcinoma by high-intensity focused ultrasound. World J Gastroenterol 2010; 16: 3584–3591.
183. Ma J, Yuan H, Zhang J, Sun X, Yi L, Li W, *et al.* An ultrasound-activated nanoplatform remodels tumor microenvironment through diverse cell death induction for improved immunotherapy. J Control Release 2024; 370: 501-515.
184. Sethuraman SN, Singh MP, Patil G, Li S, Fiering S, Hoopes PJ, *et al.* Novel calreticulin-nanoparticle in combination with focused ultrasound induces immunogenic cell death in melanoma to enhance antitumor immunity. Theranostics 2020; 10: 3397-3412.
185. von Eckstaedt H V, Weng K, Sacksen I, Stovall R, Grivas P, Bhatia S, *et al.* Sonographic signatures of immune checkpoint inhibitor-associated musculoskeletal adverse events. Cancers 2025; 17: 2344.
186. Abe S, Nagata H, Crosby EJ, Inoue Y, Kaneko K, Liu CX, *et al.* Combination of ultrasound-based mechanical disruption of tumor with immune checkpoint blockade modifies tumor microenvironment and augments systemic antitumor immunity. J Immunother Cancer 2022; 10: e003717.
187. Yilmaz M, Karaaslan M, Şirin ME, Aybal HÇ, Polat ME, Soyturk S, *et al.* Efficacy of low-intensity pulsed ultrasound (LIPUS) in the treatment of erectile dysfunction: A systematic review. Int Urol Nephrol 2025; 58: 77-89.
188. Bai Y, Li X, Wu K, Heng BC, Zhang X, Deng X. Biophysical stimuli for promoting bone repair and regeneration. 2025; 5: 1-22.
189. Kearney CJ, Hsu HP, Spector M. The use of extracorporeal shock wave-stimulated periosteal cells for orthotopic bone generation. Tissue Eng Part A 2012; 18: 1500–1508.
190. Wu S, Xu X, Sun J, Zhang Y, Shi J, Xu T. Low-intensity pulsed ultrasound accelerates traumatic vertebral fracture healing by coupling proliferation of type H microvessels. J Ultrasound Med 2018; 37: 1733–1742.
191. Wang X, Lin Q, Zhang T, Wang X, Cheng K, Gao M, *et al.* Low-intensity pulsed ultrasound promotes chondrogenesis of mesenchymal stem cells via regulation of autophagy. Stem Cell Res Ther 2019; 10: 41.
192. Liao Q, Li BJ, Li Y, Xiao Y, Zeng H, Liu JM, *et al.* Low-intensity pulsed ultrasound promotes osteoarthritic cartilage regeneration by BMSC-derived exosomes via modulating the NF-κB signaling pathway. Int Immunopharmacol 2021; 97: 107824.
193. Zhou J, Zhu Y, Ai D, Zhou M, Li H, Fu Y, *et al.* Low-intensity pulsed ultrasound regulates osteoblast-osteoclast crosstalk via EphrinB2/EphB4 signaling for orthodontic alveolar bone remodeling. Front Bioeng Biotechnol 2023; 11: 1192720.
194. Ying S, Tan M, Feng G, Kuang Y, Chen D, Li J, *et al.* Low-intensity pulsed ultrasound regulates alveolar bone homeostasis in experimental periodontitis by diminishing oxidative stress. Theranostics 2020; 10: 9789–9807.
195. Teoh KH, Whitham R, Wong JF, Hariharan K. The use of low-intensity pulsed ultrasound in treating delayed union of fifth metatarsal fractures. Foot (Edinb) 2018; 35: 52–55.
196. Schofer MD, Block JE, Aigner J, Schmelz A. Improved healing response in delayed unions of the tibia with low-intensity pulsed ultrasound: Results of a randomized sham-controlled trial. BMC Musculoskelet Disord 2010; 11: 229.
197. Farkash U, Bain O, Gam A, Nyska M, Sagiv P. Low-intensity pulsed ultrasound for treating delayed union scaphoid fractures: Case series. J Orthop Surg Res 2015; 10: 72.
198. Simpson A, Keenan G, Nayagam S, Atkins RM, Marsh D, Clement ND. Low-intensity pulsed ultrasound does not influence bone healing by distraction osteogenesis: a multicentre double-blind randomised control trial. Bone Joint J 2017; 99: 494–502.
199. Salem KH, Schmelz A. Low-intensity pulsed ultrasound shortens the treatment time in tibial distraction osteogenesis. Int Orthop 2014; 38: 1477–1482.
200. Sun S, Tang L, Zhao T, Kang Y, Sun L, Liu C, *et al.* Longitudinal effects of low-intensity pulsed ultrasound on osteoporosis and osteoporotic bone defect in ovariectomized rats. Ultrasonics 2021; 113: 106360.
201. Wada K, Kawano M, Hemmi Y, Suzuki R, Kunoki K, Sakagami H, *et al.* Effect of low-intensity pulsed ultrasound on healing of bone defects in rat tibia as measured by reconstructed three-dimensional analysis of micro CT images. *In Vivo* 2022; 36: 643–648.
202. Wang Y, Qiu Y, Li J, Zhao C, Song J. Low-intensity pulsed ultrasound promotes alveolar bone regeneration in a periodontal injury model. Ultrasonics 2018; 90: 166–172.
203. Zeng Q, Qi X, Shi G, Zhang M, Haick H. Wound dressing: From nanomaterials to diagnostic dressings and healing evaluations. ACS Nano 2022; 16: 1708–1733.
204. Zhao Y, Wang S, Ding Y, Zhang Z, Huang T, Zhang Y, *et al.* Piezotronic effect-augmented Cu(2-x)O-BaTiO(3) sonosensitizers for multifunctional cancer dynamic therapy. ACS Nano 2022; 16: 9304–9316.
205. Pang Y, He X, Qiu Z, Zhang H, Xie R, Liu Z, *et al.* Targeting integrin pathways: Mechanisms and advances in therapy. Signal Transduct Target Ther 2023; 8: 1.
206. Chaudhuri O, Cooper-White J, Janmey PA, Mooney DJ, Shenoy VB. Effects of extracellular matrix viscoelasticity on cellular behaviour. Nature 2020; 584: 535–546.
207. Xia P, Shen S, Lin Q, Cheng K, Ren S, Gao M, *et al.* Low-intensity pulsed ultrasound treatment at an early osteoarthritis stage protects rabbit cartilage from damage via the integrin/focal adhesion kinase/mitogen-activated protein kinase signaling pathway. J Ultrasound Med 2015; 34: 1991–1999.
208. Pascoal S, Monteiro F, Oliveira S, Simoni A, Carvalho Ó, Pinho T. Biomodulation effects induced by ultrasound stimulation in periodontal cells implicated in orthodontic tooth movement: A systematic review. Orthod Craniofac Res 2025; 28: 54–66.
209. Jing L, Fan S, Yao X, Zhang Y. Effects of compound stimulation of fluid shear stress plus ultrasound on stem cell proliferation and osteogenesis. Regen Biomater 2021; 8: rbab066.
210. Zhang G, Li X, Wu L, Qin YX. Piezo1 channel activation in response to mechanobiological acoustic radiation force in osteoblastic cells. Bone Res 2021; 9: 16.
211. Zhou H, Dong Y, Wu Z, Peng X, Yan M, Chen S, *et al.* Ultrasound-assisted enzyme extraction of dendrobium officinale polysaccharides: Extraction process, characterization, immunomodulatory effects. Ultrason Sonochem 2025; 114: 107248.
212. Svenskaya YI, Genina EA, Parakhonskiy B V, Lengert E V, Talnikova EE, Terentyuk GS, *et al.* A simple non-invasive approach toward efficient transdermal drug delivery based on biodegradable particulate system. ACS Appl Mater Interfaces 2019; 11: 17270-17282.
213. Su M, Li C, Deng S, Xu L, Shan Z, Xing Y, *et al.* Balance between the CMC/ACP nanocomplex and blood assimilation orchestrates immunomodulation of the biomineralized collagen matrix. ACS Appl Mater Interfaces 2023; 15: 58166–58180.
214. Newton JM, Hanoteau A, Liu HC, Gaspero A, Parikh F, Gartrell-Corrado RD, *et al.* Immune microenvironment modulation unmasks therapeutic benefit of radiotherapy and checkpoint inhibition. J Immunother Cancer 2019; 7: 216.
215. Hoefsmit EP, Rozeman EA, Van TM, Dimitriadis P, Krijgsman O, Conway JW, *et al.* Comprehensive analysis of cutaneous and uveal melanoma liver metastases. J Immunother Cancer 2020; 8: e001501.

216. Reilley MJ, Morrow B, Ager CR, Liu A, Hong DS, Curran MA. TLR9 activation cooperates with T cell checkpoint blockade to regress poorly immunogenic melanoma. J Immunother Cancer 2019; 7: 323.
217. Tang S, Tang R, Chen G, Zhang D, Lin K, Yang H, *et al.* Personalized neoantigen hydrogel vaccine combined with PD-1 and CTLA-4 double blockade elicits antitumor response in liver metastases by activating intratumoral $CD8^{+}CD69^{+}$ T cells. J Immunother Cancer 2024; 12: e009543.
218. Xu J, Wang H, Xu L, Chao Y, Wang C, Han X, *et al.* Nanovaccine based on a protein-delivering dendrimer for effective antigen cross-presentation and cancer immunotherapy. Biomaterials 2019; 207: 1-9.
219. Gou S, Wang S, Liu W, Chen G, Zhang D, Du J, *et al.* Adjuvant-free peptide vaccine targeting Clec9a on dendritic cells can induce robust antitumor immune response through Syk/IL-21 axis. Theranostics 2021; 11: 7308-7321.
220. Yan S, Wang D, Zhang L, Gan T, Yao H, Zhu H, *et al.* LIPUS-S/B@NPs regulates the release of SDF-1 and BMP-2 to promote stem cell recruitment-osteogenesis for periodontal bone regeneration. Front Bioeng Biotechnol 2023; 11: 1226426.
221. Zhang N, Chow SKH, Leung KS, Cheung WH. Ultrasound as a stimulus for musculoskeletal disorders. J Orthop Transl 2017; 9: 52–59.
222. Butler S, Ashcroft K, Arrowsmith S, Griffiths R, Studd A. Assessment of thermal index compliance in clinical ultrasound examinations. Ultrasound 2024; 32: 151–156.
223. Wu J, Xie F, Lof J, Sayyed S, Porter TR. Utilization of modified diagnostic ultrasound and microbubbles to reduce myocardial infarct size. Heart 2015; 101: 1468–1474.
224. Drukker L, Droste R, Chatelain P, Noble JA, Papageorghiou AT. Safety indices of ultrasound: Adherence to recommendations and awareness during routine obstetric ultrasound scanning. Ultraschall Med 2020; 41: 138–145.
225. Abbott JG. Rationale and derivation of MI and TI—a review. Ultrasound Med Biol 1999; 25: 431–441.
226. Zhu Y, Zhang Q, Wang Y, Liu W, Zeng S, Yuan Q, *et al.* Identification of necroptosis and immune infiltration in heart failure through bioinformatics analysis. J Inflamm Res 2025; 18: 2465–2481.
227. Lentacker I, De Cock I, Deckers R, De Smedt SC, Moonen CTW. Understanding ultrasound induced sonoporation: Definitions and underlying mechanisms. Adv Drug Deliv Rev 2014; 72: 49–64.
228. Tomizawa M, Shinozaki F, Motoyoshi Y, Sugiyama T, Yamamoto S, Sueishi M. Sonoporation: Gene transfer using ultrasound. World J Methodol 2013; 3: 39–44.
229. Liang J, Chen L, Li Y, Chen Y, Yuan L, Qiu Y, *et al.* Unraveling the prefrontal cortex-basolateral amygdala pathway's role on schizophrenia's cognitive impairments: A multimodal study in patients and mouse models. Schizophr Bull 2024; 50: 913–923.
230. Birdi J, Heymans S V., Collado-Lara G, Van Den Abeele K, D'hooge J, Bertrand A. Single-shot attenuation coefficient estimation for ultrasound contrast agents. Front Phys 2022; 10: 1-21.
231. Bao MH, Lv QL, Li HG, Zhang YW, Xu BF, He BS. A novel putative role of TNK1 in atherosclerotic inflammation implicating the Tyk2/STAT1 pathway. Mediators Inflamm 2020; 2020: 6268514.
232. Elmekki H, Islam S, Alagha A, Sami H, Spilkin A, Zakeri E, *et al.* Comprehensive review of reinforcement learning for medical ultrasound imaging. Artif Intell Rev 2025; 58: 284.
233. Ting SG, Lea-Banks H, Hynynen K. Physical characterization to improve scalability and potential of anesthetic-loaded nanodroplets. Pharmaceutics 2023; 15: 2077.
234. Martin KH, Dayton PA. Current status and prospects for microbubbles in ultrasound theranostics. Wiley Interdiscip Rev Nanomed Nanobiotechnol 2013; 5: 329–345.
235. Gawne PJ, Ferreira M, Papaluca M, Grimm J, Decuzzi P. New opportunities and old challenges in the clinical translation of nanotheranostics. Nat Rev Mater 2023; 8: 783–798.
236. Kiessling F, Fokong S, Koczera P, Lederle W, Lammers T. Ultrasound microbubbles for molecular diagnosis, therapy, and theranostics. J Nucl Med 2012; 53: 345–348.
237. Stern AD. Innovation under regulatory uncertainty: Evidence from medical technology. J Public Econ. 2017; 145: 181–200.
238. Kiessling F, Fokong S, Bzyl J, Lederle W, Palmowski M, Lammers T. Recent advances in molecular, multimodal and theranostic ultrasound imaging. Adv Drug Deliv Rev 2014; 72: 15-27.
239. Oddo L, Cerroni B, Domenici F, Bedini A, Bordi F, Chiessi E, *et al.* Next generation ultrasound platforms for theranostics. J Colloid Interface Sci 2017; 491: 151–160.
240. Yan L, Li Q, Fu K, Zhou X, Zhang K. Progress in the application of artificial intelligence in ultrasound-assisted medical diagnosis. Bioeng (Basel, Switzerland) 2025; 12: 288.
241. Chen Y, Yang H, Pan H, Siddiqui F, Verdone A, Zhang Q, *et al.* BURExtract-Llama: An LLM for Clinical Concept Extraction in Breast Ultrasound Reports. In: Proceedings of the 1st International Workshop on Multimedia Computing for Health and Medicine. New York, NY, USA: Association for Computing Machinery; 2024. p. 53-58.
242. Xu X, Sankar R. Large language model agents for biomedicine: a comprehensive review of methods, evaluations, challenges, and future directions. Information 2025; 16: 894.
243. Wang C, He T, Zhou H, Zhang Z, Lee C. Artificial intelligence enhanced sensors - enabling technologies to next-generation healthcare and biomedical platform. Bioelectron Med 2023; 9: 17.
244. Puccetti M, Pariano M, Schoubben A, Giovagnoli S, Ricci M. Biologics, theranostics, and personalized medicine in drug delivery systems. Pharmacol Res 2024; 201: 107086.
245. Zou T, Liu Y, Luo Y, Xu T. A wearable spatiotemporal controllable ultrasonic device with amyloid-β disaggregation for continuous Alzheimer's disease therapy. Sci Adv 2025; 11: eadw1782.
246. Sergeeva O V., Luo L, Guiseppi-Elie A. Cancer theragnostics: Closing the loop for advanced personalized cancer treatment through the platform integration of therapeutics and diagnostics. Front Bioeng Biotechnol 2025; 12: 1499474.
247. Xie R, Wang Y, Gong S. External stimuli-responsive nanoparticles for spatially and temporally controlled delivery of CRISPR-Cas genome editors. Biomater Sci 2021; 9: 6012–6022.
248. Liu Z, Si L, Shi S, Li J, Zhu J, Lee WH, *et al.* Classification of three anesthesia stages based on near-infrared spectroscopy signals. IEEE J Biomed Heal informatics 2024; 28: 5270–5279.
249. Hu F, Yang H, Qiu L, Wang X, Ren Z, Wei S, *et al.* Innovation networks in the advanced medical equipment industry: Supporting regional digital health systems from a local-national perspective. Front public Heal 2025; 13: 1635475.
250. Johanssen VA, Ruan JL, Vince O, Thomas A, Peeters S, Soto MS, *et al.* Targeted opening of the blood-brain barrier using VCAM-1 functionalised microbubbles and "whole brain" ultrasound. Theranostics 2024; 14: 4076–4089.
251. Kaufmann BA, Sanders JM, Davis C, Xie A, Aldred P, Sarembock IJ, *et al.* Molecular imaging of inflammation in atherosclerosis with targeted ultrasound detection of vascular cell adhesion molecule-1. Circulation 2007; 116: 276–284.
252. Langbein T, Weber WA, Eiber M. Future of theranostics: An outlook on precision oncology in nuclear medicine. J Nucl Med 2019; 60: 13S-19S.
253. Pandit-Taskar N, Modak S. Norepinephrine transporter as a target for imaging and therapy. J Nucl Med 2017; 58: 39S-53S.
254. Gawne PJ, Bryant HE, DuBois SG, George SL, Gray J, Knox L, *et al.* Theranostics for neuroblastoma: Making molecular radiotherapy work better. J Nucl Med 2025; 66: 490–496.
255. Eberlein U, Cremonesi M, Lassmann M. Individualized dosimetry for theranostics: necessary, nice to have, or counterproductive? J Nucl Med 2017; 58: 97S-103S.
256. Nagarajah J, Janssen M, Hetkamp P, Jentzen W. Iodine symporter targeting with (124)I/(131)I theranostics. J Nucl Med

2017; 58: 34S-38S.
257. Lin G, Mu Q, Revia R, Stephen Z, Jeon M, Zhang M. A highly selective iron oxide-based imaging nanoparticle for long-term monitoring of drug-induced tumor cell apoptosis. Biomater Sci 2021; 9: 471–481.
258. Jiang F, Liu S, Wang L, Chen H, Huang Y, Cao Y, *et al.* ROS-responsive nanoprobes for bimodal imaging-guided cancer targeted combinatorial therapy. Int J Nanomedicine 2024; 19: 8071–8090.
259. Jolesz FA. MRI-guided focused ultrasound surgery. Annu Rev Med 2009; 60: 417–430.
260. Shen YT, Chen L, Yue WW, Xu HX. Artificial intelligence in ultrasound. Eur J Radiol 2021; 139: 109717.
261. Du Y, Chen L, Yan MC, Wang YL, Zhong XL, Xv CX, *et al.* Neurometabolite levels in the brains of patients with autism spectrum disorders: A meta-analysis of proton magnetic resonance spectroscopy studies (N = 1501). Mol Psychiatry 2023; 28: 3092-3103.
262. Kayarian F, Patel D, O'Brien JR, Schraft EK, Gottlieb M. Artificial intelligence and point-of-care ultrasound: Benefits, limitations, and implications for the future. Am J Emerg Med 2024; 80: 119–122.
263. Jiang Y, Zhang L, Liu Z, Wang L. The value of handheld ultrasound in point-of-care or at home EF prediction. Acta Cardiol 2025; 80: 979-985.
264. Chen L, Jiang Z, Yang L, Fang Y, Lu S, Akakuru OU, *et al.* HPDA/Zn as a CREB inhibitor for ultrasound imaging and stabilization of atherosclerosis plaque. Chinese J Chem 2023; 41: 199–206.
265. Kim S, Fischetti C, Guy M, Hsu E, Fox J, Young SD. Artificial intelligence (AI) applications for point of care ultrasound (POCUS) in low-resource settings: A scoping review. Diagnostics (Basel, Switzerland) 2024; 14: 1669.
266. Akkus Z, Cai J, Boonrod A, Zeinoddini A, Weston AD, Philbrick KA, *et al.* A survey of deep-learning applications in ultrasound: Artificial intelligence–powered ultrasound for improving clinical workflow. J Am Coll Radiol 2019; 16: 1318-1328.
267. Luan S, Yu X, Lei S, Ma C, Wang X, Xue X, *et al.* Deep learning for fast super-resolution ultrasound microvessel imaging. Phys Med Biol 2023; 68: 245023.
268. Yu X, Luan S, Lei S, Huang J, Liu Z, Xue X, *et al.* Deep learning for fast denoising filtering in ultrasound localization microscopy. Phys Med Biol 2023; 68: 205002.
269. Li B, Enichen EJ, Heydari K, Kvedar JC. Artificial intelligence guided imaging as a tool to fill gaps in health care delivery. NPJ Digit Med 2025; 8: 248.
270. Liu Z, Li M, Xie Q, Liu Y, Huang J, Zeng Q, *et al.* Eradicating fungal biofilm-based infections by ultrasound-assisted semiconductor sensitized upconversion photodynamic therapy. Nat Commun 2025; 16: 6499.
271. Baloescu C, Bailitz J, Cheema B, Agarwala R, Jankowski M, Eke O, *et al.* Artificial intelligence-guided lung ultrasound by nonexperts. JAMA Cardiol 2025; 10: 245-253.
272. Komatsu M, Sakai A, Dozen A, Shozu K, Yasutomi S, Machino H, *et al.* Towards clinical application of artificial intelligence in ultrasound imaging. Biomedicines 2021; 9: 720.
273. Wu GG, Zhou LQ, Xu JW, Wang JY, Wei Q, Deng YB, *et al.* Artificial intelligence in breast ultrasound. World J Radiol 2019; 11: 19-26.
274. Jiang Z, Chen Z, Xu Y, Li H, Li Y, Peng L, *et al.* Low-frequency ultrasound sensitive piezo1 channels regulate keloid-related characteristics of fibroblasts. Adv Sci 2024; 11: e2305489.
275. García-Herreros S, López Gómez JJ, Cebria A, Izaola O, Salvador Coloma P, Nozal S, *et al.* Validation of an artificial intelligence-based ultrasound imaging system for quantifying muscle architecture parameters of the rectus femoris in disease-related malnutrition (DRM). Nutrients 2024; 16: 1806.
276. Firuzpour F, Saleki K, Aram C, Rezaei N. Nanocarriers in glioblastoma treatment: A neuroimmunological perspective. Rev Neurosci 2024; 36: 431-453.
277. Rahimi M, Fattahi A. Acidity enhancement of α-carbon of beta diketones via hydroxyl substituents: A density functional theory study. J Phys Org Chem 2021; 34: e4157.
278. Omata D, Unga J, Suzuki R, Maruyama K. Lipid-based microbubbles and ultrasound for therapeutic application. Adv Drug Deliv Rev 2020; 154–155: 236–44.
279. Aram C, Firuzpour F, Parancheshmeh M, Kamali MJ. Unveiling the translational and therapeutic potential of small interfering RNA molecules in combating SARS-CoV-2: A review. Int J Biol Macromol 2025; 318: 145203.
280. Cai L, Pfob A. Artificial intelligence in abdominal and pelvic ultrasound imaging: Current applications. Abdom Radiol 2025; 50: 1775–1789.
281. Vonken R. Cardiac ultrasound uses artificial intelligence to produce images. JAMA 2020; 323: 1034.
282. Fraga S, Brandão A, Soares ME, Morais T, Duarte JA, Pereira L, *et al.* Short- and long-term distribution and toxicity of gold nanoparticles in the rat after a single-dose intravenous administration. Nanomedicine 2014; 10: 1757–1766.
283. Zhang XD, Luo Z, Chen J, Song S, Yuan X, Shen X, *et al.* Ultrasmall glutathione-protected gold nanoclusters as next generation radiotherapy sensitizers with high tumor uptake and high renal clearance. Sci Rep 2015; 5: 8669.
284. Ali MRK, Rahman MA, Wu Y, Han T, Peng X, Mackey MA, *et al.* Efficacy, long-term toxicity, and mechanistic studies of gold nanorods photothermal therapy of cancer in xenograft mice. Proc Natl Acad Sci 2017; 114: E3110–3118.
285. Wang X, Xie N, Zhang H, Zhou W, Lei J. Isoorientin ameliorates macrophage pyroptosis and atherogenesis by reducing KDM4A levels and promoting SKP1-Cullin1-F-box E3 ligase-mediated NLRP3 ubiquitination. Inflammation 2025; 48: 3629-3648.
286. Chen L, Cruz E, Oikari LE, Padmanabhan P, Song J, Götz J. Opportunities and challenges in delivering biologics for Alzheimer's disease by low-intensity ultrasound. Adv Drug Deliv Rev 2022; 189: 114517.
287. Wan Y, Shen Y, Wang J, Zhang T, Fu X. Knowledge mapping of ultrasound technology and triple-negative breast cancer: A visual and bibliometric analysis. Discov Oncol 2025; 16: 1248.